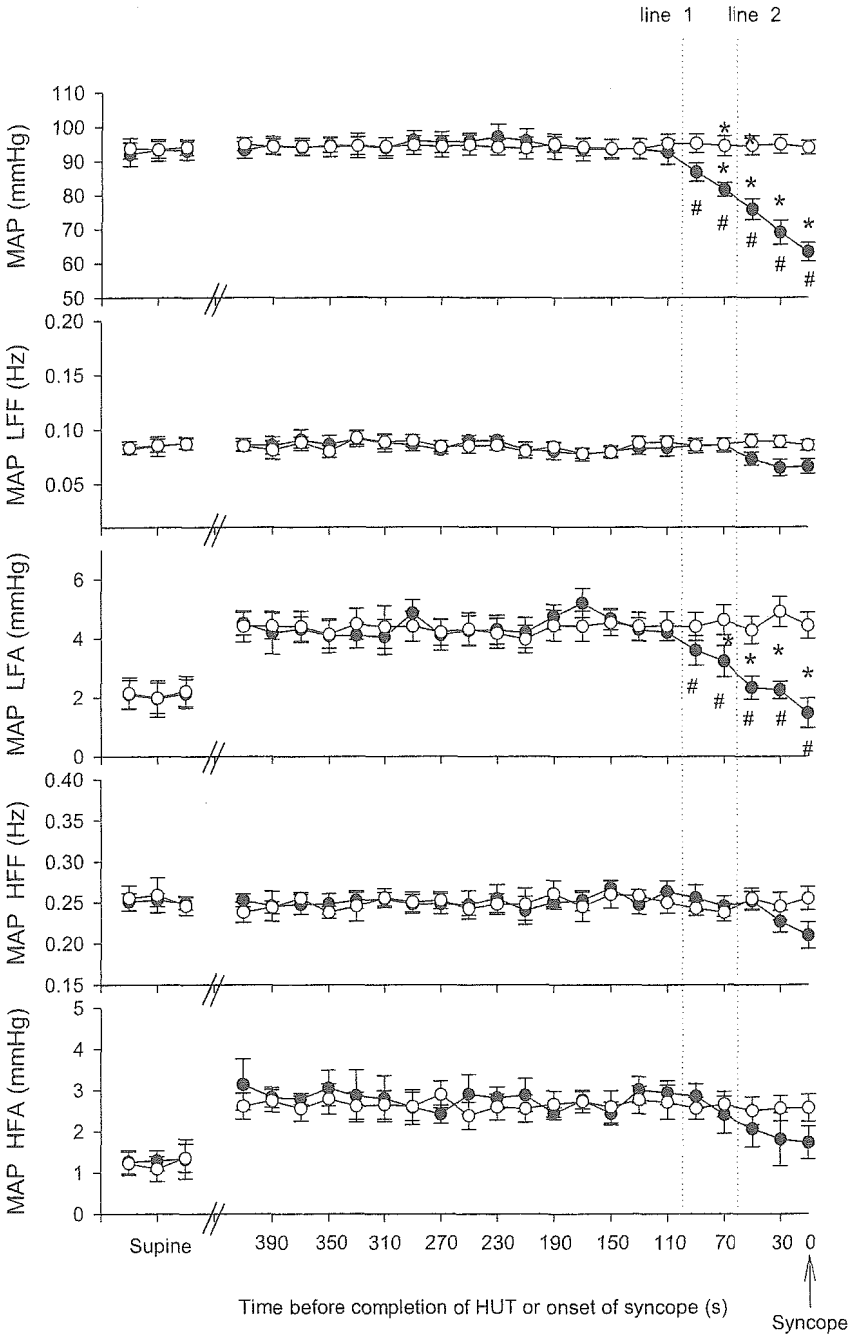

Fig. 3. Mean AP (MAP), frequency of LF component of MAP variability (MAP LFF), amplitude of LF component of SAP variability (MAP LFA), frequency of HF component of SAP variability (MAP HFF), and amplitude of HF component of MAP variability (MAP HFA) in syncopal (●) and nonsyncopal (○) subjects during 6 min of supine rest (averaged every 2 min) and during 410 s before completion of HUT test or onset of syncope in HUT (averaged every 20s). LF and HF amplitudes in both groups are higher throughout HUT than in supine posture ($P < 0.05$), except LF in the syncopal group, which is higher only until 60 s before onset of syncope ($P < 0.05$). $^{*}P < 0.05$, syncopal vs. nonsyncopal. $^{\#}P < 0.05$ vs. mean for the first 100 s of HUT. Error bars, SE.

as LF and HF amplitudes of their variability, were similar in nonsyncopal and syncopal groups (Figs. 2–5). Respiratory rates were also similar in the two groups. LF oscillation of MSNA and the mirrored oscillation in AP are clearly demonstrated in the representative recording (Fig. 1).

From 100 s before onset of syncope, AP (systolic, diastolic, and mean) started to decrease, and LF oscillation of MSNA weakened, as shown in the representative recording in Fig. 1. Data from all subjects showed that, from 100 to 60 s before onset of syncope, LF amplitude of MSNA variability started to decrease (Fig. 4). In contrast, magnitudes of MSNA (burst rate and total activity) and HF amplitude of MSNA variability remained elevated above 0° supine levels (Fig. 4; $P < 0.05$). AP (systolic, diastolic, and mean) started to decrease, but pulse pressure did not change (Fig. 2). LF amplitude of mean AP variability started to decrease, whereas HF amplitude of the variability remained increased above 0° supine levels (Fig. 3; $P < 0.05$). R-R interval and HF amplitude of R-R interval variability remained decreased below 0° supine levels (Fig. 5; $P < 0.05$). Respiratory rate was nearly constant at 15 cycles/min. Instantaneous frequencies in LF and HF bands of all variables remained fixed at ~0.09 and 0.25 Hz, respectively (Figs. 2–5).

From 60 s before to onset of syncope, AP (systolic, diastolic, and mean) further decreased (Fig. 2). Pulse pressure decreased in the last 20 s (Fig. 2). LF amplitude of MSNA variability further decreased (Fig. 4). Magnitudes of MSNA (burst rate and total activity) decreased markedly (Fig. 4), as seen in the representative recording in Fig. 1. HF amplitude of MSNA

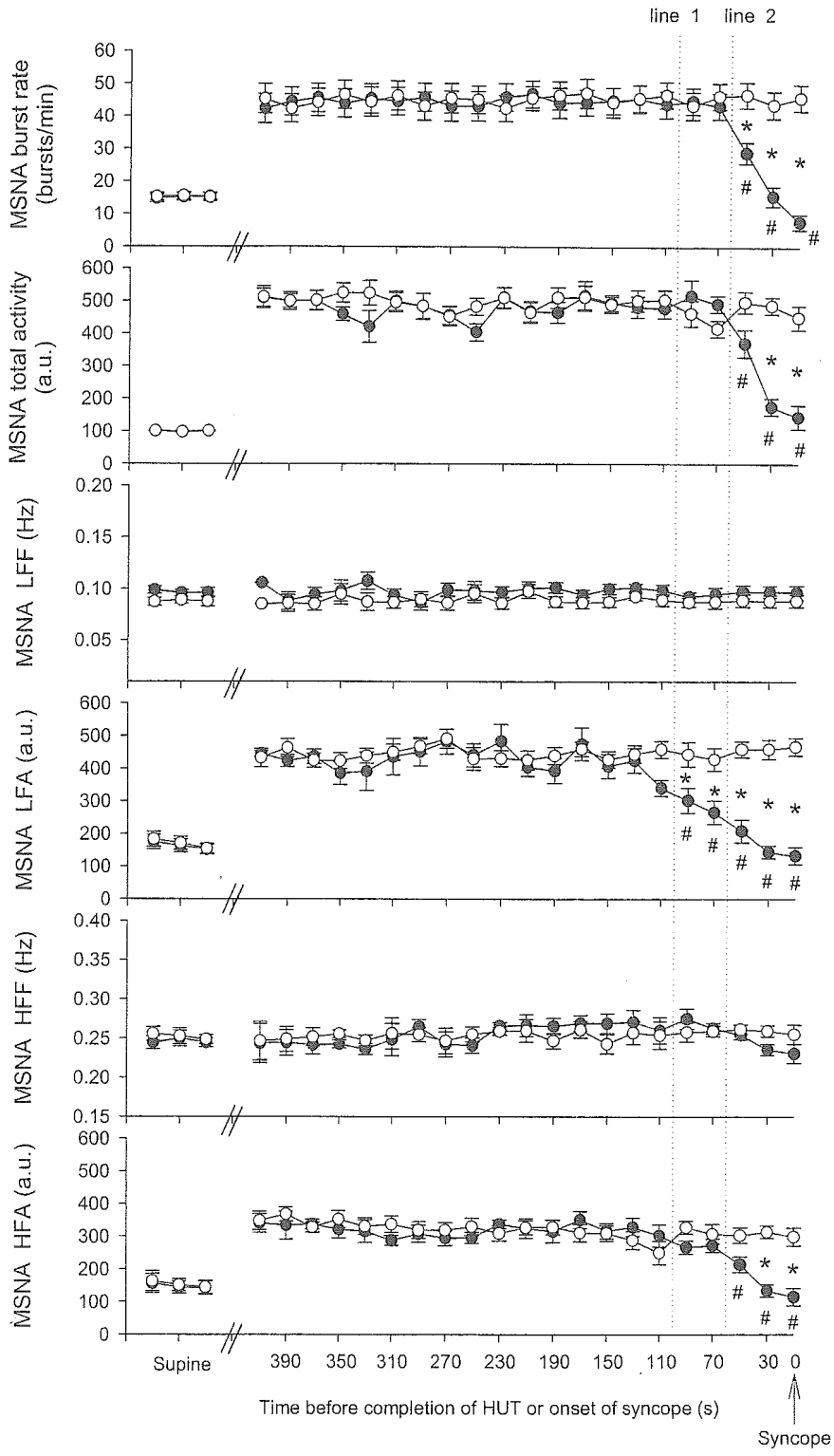

Fig. 4. Muscle sympathetic nerve activity (MSNA) burst rate, MSNA total activity, frequency of LF component of MSNA variability (MSNA LFF), amplitude of LF component of MSNA variability (MSNA LFA), frequency of HF component of MSNA variability (MSNA HFF), and amplitude of HF component of MSNA variability (MSNA HFA) in syncopal (●) and nonsyncopal (○) subjects during 6 min of supine rest (averaged every 2 min) and during 410 s before completion of HUT test or onset of syncope in HUT (averaged every 20 s). LF and HF amplitudes in nonsyncopal subjects are higher throughout HUT than in supine posture ($P < 0.05$). In contrast, LF and HF amplitudes in syncopal subjects are higher until 100 and 60 s, respectively, before onset of syncope in HUT test. $^{*}P < 0.05$, syncopal vs. nonsyncopal. $^{\#}P < 0.05$ vs. mean for the first 100 s of HUT. Error bars, SE.

variability decreased (Fig. 4). LF amplitude of mean AP variability further decreased, whereas HF amplitude of the variability remained elevated above 0° supine levels (Fig. 3; $P < 0.05$). R-R interval and LF and HF components of R-R interval variability greatly increased (Fig. 5). Respiratory rate was nearly constant at 15 cycles/min. Instantaneous frequencies for LF and HF bands of all variables remained fixed at ~0.09 and 0.25 Hz, respectively (Fig. 2–5).

Coherence function. In the LF band, MSNA exhibited coherence with the R-R interval and AP during 0° supine rest and significantly stronger coherence during HUT in syncopal and nonsyncopal subjects (Table 1). In the HF band, MSNA exhibited coherence with the R-R interval, AP, and respiration during 0° supine rest and coherence did not change during HUT in syncopal and nonsyncopal subjects (Table 1).

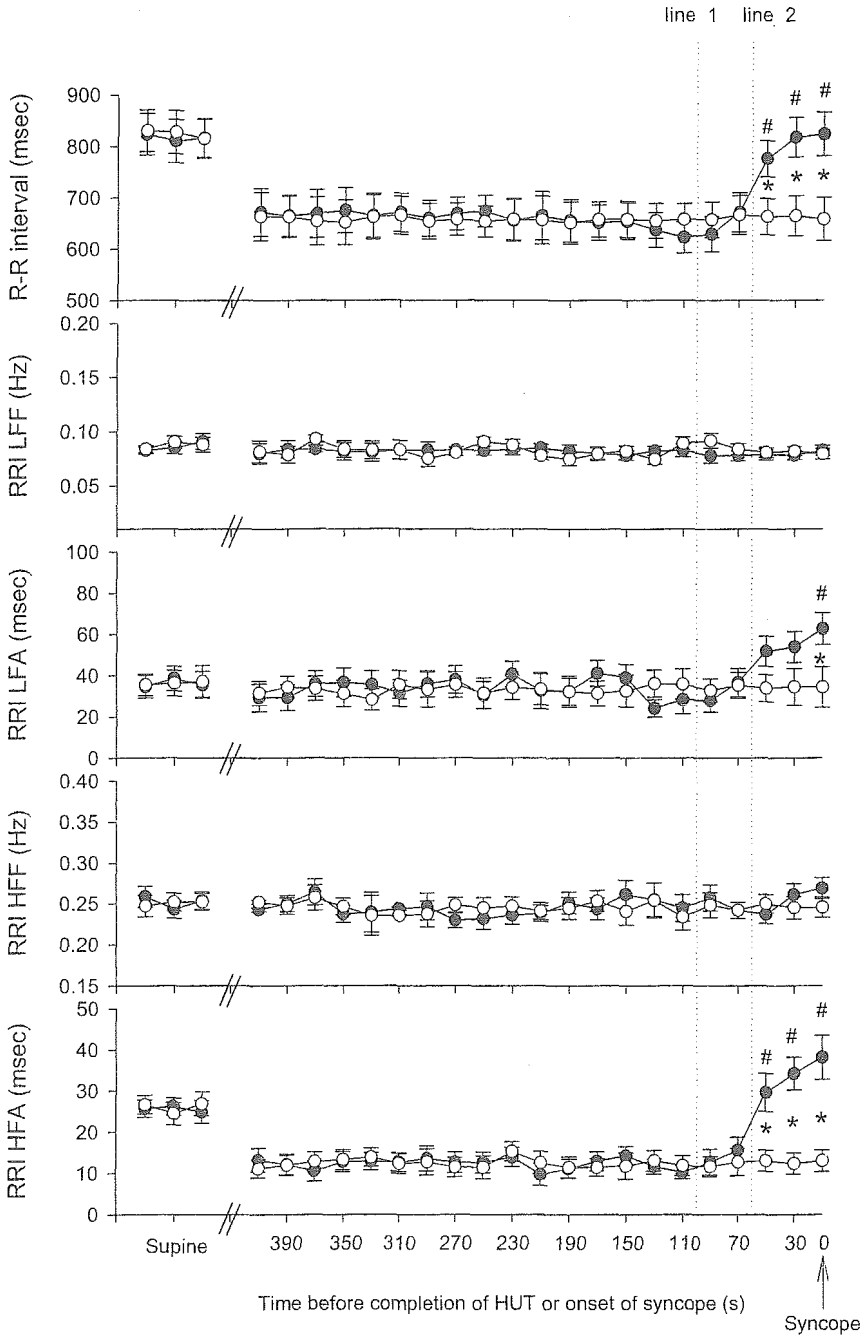

Fig. 5. R-R interval (RRI), frequency of LF component of RRI variability (RRI LFF), amplitude of LF component of RRI variability (RRI LFA), frequency of HF component of RRI variability (RRI HFF), and amplitude of HF component of RRI variability (RRI HFA) in syncopal (●) and nonsyncopal (○) subjects during 6 min of supine rest (averaged every 2 min) and for 410 s before completion of HUT test or onset of syncope in HUT (averaged every 20 s). LF amplitude in both groups is similar throughout HUT compared with supine posture, except at the last HUT time point in syncopal subjects, when it is higher than in supine posture ($P < 0.05$). HF amplitude in both groups is lower throughout HUT than in supine posture ($P < 0.05$), except at the last HUT time point in syncopal subjects, when it is higher ($P < 0.05$). *$P < 0.05$, syncopal vs. nonsyncopal. #$P < 0.05$ vs. mean for the first 100 s of HUT. Error bars, SE.

DISCUSSION

Orthostatic sympathetic activation plays a crucial role in maintaining AP under orthostatic stress. Sympathetic activation is accompanied by marked LF oscillation of SNA variability. However, because LF oscillation of MSNA has been investigated only in steady-state orthostasis, when AP is well maintained, LF oscillation during the course of development of orthostatic neurally mediated syncope remains unknown. We used complex demodulation to assess nonstationary time-dependent changes in MSNA variability in 10 healthy subjects in whom neurally mediated syncope was evoked by HUT. In agreement with earlier studies (16–18), our present data show that orthostatic neurally mediated syncope was accompanied by a marked reduction of MSNA. Our new major finding is that LF oscillation of MSNA decreased during development of orthostatic neurally mediated syncope. Unexpectedly, the decrease in LF oscillation of MSNA preceded the reduction in magnitudes of MSNA. The result supports our hypothesis that LF oscillation of SNA decreases during orthostatic neurally mediated syncope.

As far as we are aware, the present study is the first that addresses the time course of changes in MSNA oscillation in development of orthostatic neurally mediated syncope. The change in MSNA oscillation consisted of two stages. The first stage (from 100 to 60 s before onset of syncope) is marked by a decrease in LF oscillation of MSNA at the initial development of orthostatic neurally mediated syncope, when AP starts to decrease. MSNA and heart rate remain elevated above horizontally supine levels. The second stage (from 60 s before to onset of

Table 1. *Coherence between MSNA and R-R interval, mean AP, and respiration during HUT in syncope and nonsyncope*

	RRI-MSNA		AP-MSNA		Resp-MSNA
	LF	HF	LF	HF	HF
			Syncope		
0° baseline	0.59±0.11	0.58±0.12	0.56±0.10	0.64±0.11	0.61±0.08
Early HUT	0.75±0.12*	0.55±0.11	0.74±0.09*	0.65±0.13	0.61±0.07
Initial development of syncope	0.72±0.11*	0.53±0.13	0.69±0.11*	0.64±0.12	0.62±0.11
Just before onset of syncope	0.67±0.11*	0.54±0.12	0.68±0.11*	0.65±0.14	0.60±0.12
			Nonsyncope		
0° baseline	0.60±0.11	0.61±0.12	0.61±0.10	0.58±0.11	0.62±0.07
Early HUT	0.72±0.10*	0.57±0.15	0.72±0.10*	0.62±0.12	0.61±0.09
Mid-HUT	0.72±0.12*	0.58±0.14	0.71±0.09*	0.59±0.13	0.58±0.08
Last HUT	0.74±0.11*	0.57±0.13	0.73±0.09*	0.61±0.12	0.59±0.09

Values are means ± SE. MSNA, muscle sympathetic nerve activity; AP, arterial pressure; HUT, head-up tilt; LF, low frequency (0.05–0.15 Hz). HF, high frequency (0.15–0.35 Hz). RRI, R-R interval; Resp, respiration. *$P < 0.05$ vs. 0° baseline.

syncope) is characterized by the total disappearance of MSNA oscillation during further development of orthostatic neurally mediated syncope, when AP further decreases to the level at syncope. Sympathetic withdrawal and bradycardia occur, consistent with earlier studies (16–18).

Increase in LF oscillations of AP and MSNA in normotensive HUT. In agreement with previous studies (1, 5), when AP was well maintained, early HUT increased the amplitude of LF oscillation of MSNA and caused mirrored changes in the amplitude of LF oscillation of mean AP (Figs. 3 and 4). In

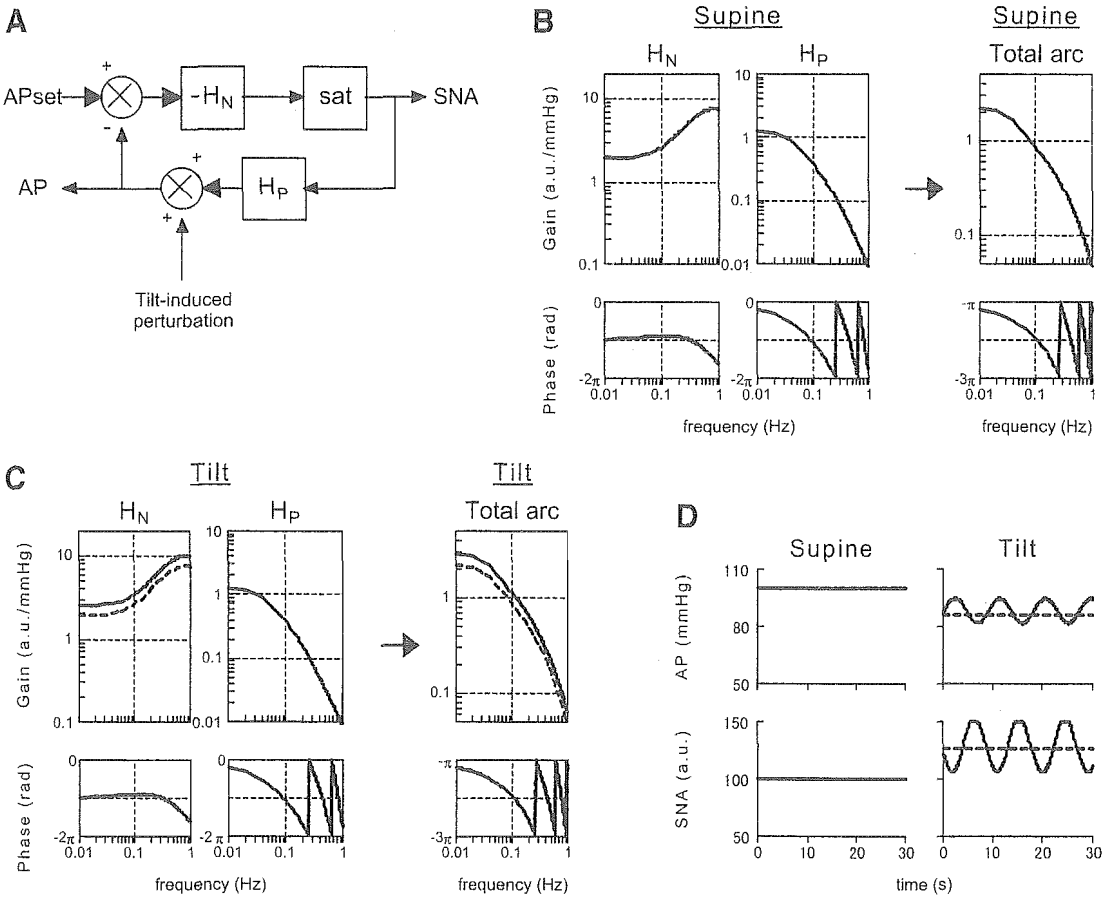

Fig. 6. Simulation of generation of LF oscillation of AP and sympathetic nerve activity (SNA) by the baroreflex theory. *A*: block diagram of total arc baroreflex system, which consists of neural arc transfer function (H_N), saturation function (sat), and neural arc transfer function (H_P). We assigned tilt-induced perturbation of −50 mmHg in simulations during HUT. We set AP_{set} at 100 mmHg and baseline SNA at 100 arbitrary units (AU) when AP = AP_{set}. *B*: H_N, H_P, and resultant total arc transfer function (shown as gain and phase) in supine posture. In the model of H_N, we set K_N at 1.9 AU/mmHg (see APPENDIX). *C*: H_N, H_P, and resultant total arc transfer function (shown as gain and phase) in tilt position. In the model of H_N, we set static gain of H_N (i.e., K_N) at 1.9 AU/mmHg (dashed line) when H_N is constant regardless of postural change (see APPENDIX). In this case, G_0 (see Fig. 7) in the total arc is <1 (dashed line). In addition, we set static gain of H_N (i.e., K_N) at 2.5 AU/mmHg (solid line) when gain of H_N increases with postural change. In this case, G_0 in the total arc is >1 (solid line). Phases are similar regardless of the increase in gain. *D*: simulated time series of AP and SNA set in *B* and *C* in supine and tilt positions. In the tilt position, simulated data show K_N = 1.9 and 2.5 AU/mmHg (dashed and solid lines, respectively). Increasing gain of H_N in the tilt position generates 0.1-Hz oscillation of AP and SNA.

addition, a high coherence between the two in the LF band was observed during HUT, consistent with results of an earlier study (5). These findings indicate that HUT induces a common LF oscillatory pattern in the variability of sympathetic discharge and AP (5).

Possible mechanism for the increase in LF oscillations of mean AP and MSNA: baroreflex-loop theory. Two mechanisms have been speculated to generate LF oscillation of mean AP and MSNA in normotensive HUT. The first mechanism is the baroreflex-loop theory (2, 6). First, we examined how the baroreflex-loop system may explain generation of LF oscillation of AP and MSNA. Figure 6*A* shows a block diagram of the arterial baroreflex system. The total arc baroreflex is a negative-feedback control system that senses AP by baroreceptors and regulates AP. The total arc baroreflex system consists of the neural arc transfer function (H_N), saturation function (sat), and peripheral arc transfer function (H_P; Fig. 6*A*) (12). H_N, coupled with saturation, represents central processing from baroreceptor pressure to SNA, whereas H_P represents processing from SNA to systemic AP. According to our previous studies, we used derivative and high-cut filter characteristics with a pure delay to model H_N and the second-order low-pass filter with a pure delay to model H_P (see APPENDIX; Fig. 6, *B* and *C*) (12). The saturation function simulates the upper and lower saturation of SNA. Because the total arc baroreflex transfer function is a multiplication of these subsystem transfer functions, it approximates a first-order low-pass filter with a pure delay, consistent with previous studies (see APPENDIX; Fig. 6, *B* and *C*) (10).

The key point of baroreflex-loop theory is whether the total arc baroreflex transfer function gain is >1 at the frequency at which the phase reaches -2π radians. The phase in the total arc transfer function is delayed as the frequency increases and reaches -2π radians at a given frequency, which we define as f_0 (Fig. 7). We also define the gain at f_0 as G_0 (Fig. 7). The total arc low-pass filter has the following important characteristics: at $G_0 > 1$, closing the feedback loop generates oscillations of AP and SNA at f_0, whereas at $G_0 < 1$, closing the loop does not generate the oscillation. Because LF oscillation of AP and SNA is not significant in the supine position, G_0 may be <1 (Fig. 6, *B* and *D*). If G_0 remains unchanged in HUT, the closed-loop baroreflex system will increase SNA in response to tilt-induced pressure perturbation by gravity but will not produce oscillation of AP and SNA (Fig. 6, *C* and *D*). However, if G_0 increases to >1 in HUT, the closed-loop baroreflex system will generate LF oscillations of AP and SNA (Fig. 6, *C* and *D*). Therefore, we raise the possibility that HUT increases G_0, resulting in generation of LF oscillations of AP and SNA.

In this baroreflex-loop model, the saturation function, which limits the magnitude of SNA, is necessary to represent the stabilized amplitude of LF oscillation of AP and MSNA observed in humans. This occurs because absence of the saturation function of SNA progressively will increase amplitudes of LF oscillations of AP and MSNA manyfold at $G_0 > 1$.

Furthermore, we can propose how the baroreflex system generates LF oscillations. Interestingly, our data showed that frequency of the LF component of AP and MSNA variability was constant in supine rest and HUT (Figs. 3 and 4). This indicates that f_0 remains unchanged during HUT. Accordingly, the possible increase in G_0 during HUT may be the result of an increase in total baroreflex transfer gain. Such an increase in total arc gain may be caused by an increase in H_N, but not H_P, gain (Fig. 6*B*). This occurs because HUT shifts body fluid toward the lower body, including the third space, and may result in deterioration of the peripheral transduction from SNA to AP.

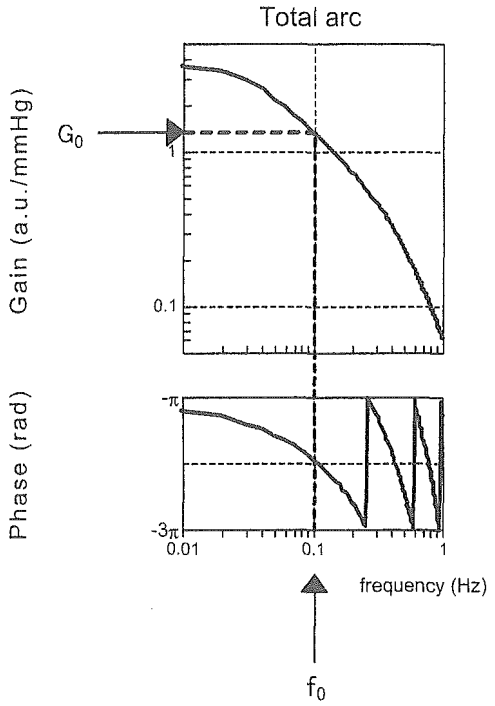

Fig. 7. Total arc transfer function obtained from the block diagram of the total arc baroreflex system (Fig. 6*A*), which approximates a 1st-order low-pass filter with a pure delay (see APPENDIX). Frequency when phase is at -2π rad is defined as f_0 and gain at f_0 as G_0. This figure shows an example when $G_0 > 1$.

Possible mechanism for increase in LF oscillations of AP and MSNA: pacemaker oscillator theory. The second mechanism that has been speculated to generate LF oscillation of AP and MSNA is the pacemaker oscillator theory (1). This theory is supported by earlier studies in dogs showing that LF oscillation of SNA persisted even after baroreceptor afferent activity was abolished by spinal section and bilateral vagotomy (11) and that LF oscillation was preserved even after baroreceptor pressure fluctuations were abolished by a pressure-stabilizing device (22). Such evidence supports the concept that the LF pacemaker oscillator generates LF oscillation of MSNA.

Next, we attempted to apply the pacemaker oscillator theory to explain LF oscillation of AP and MSNA. We added elements of the pacemaker oscillator theory to the baroreflex-feedback-loop model and modeled the pacemaker oscillator as a 0.1-Hz sine wave in a block diagram (Fig. 8*A*). The numerical simulation indicates that increasing the amplitude of SNA pacemaker oscillation will increase amplitudes of LF oscillations of MSNA and AP (Fig. 8*C*), while the baroreflex system remains constant (Fig. 8*B*). Therefore, it is possible that HUT activates the pacemaker oscillator, resulting in enhancement of LF oscillations of MSNA and AP. Details of the mechanism responsible for activation of the pacemaker oscillator are unclear.

Decrease in LF oscillations of AP and MSNA during development of tilt-induced syncope: possible involvement of baroreflex-loop and pacemaker oscillator theories. During development of tilt-induced syncope (from 100 s before to

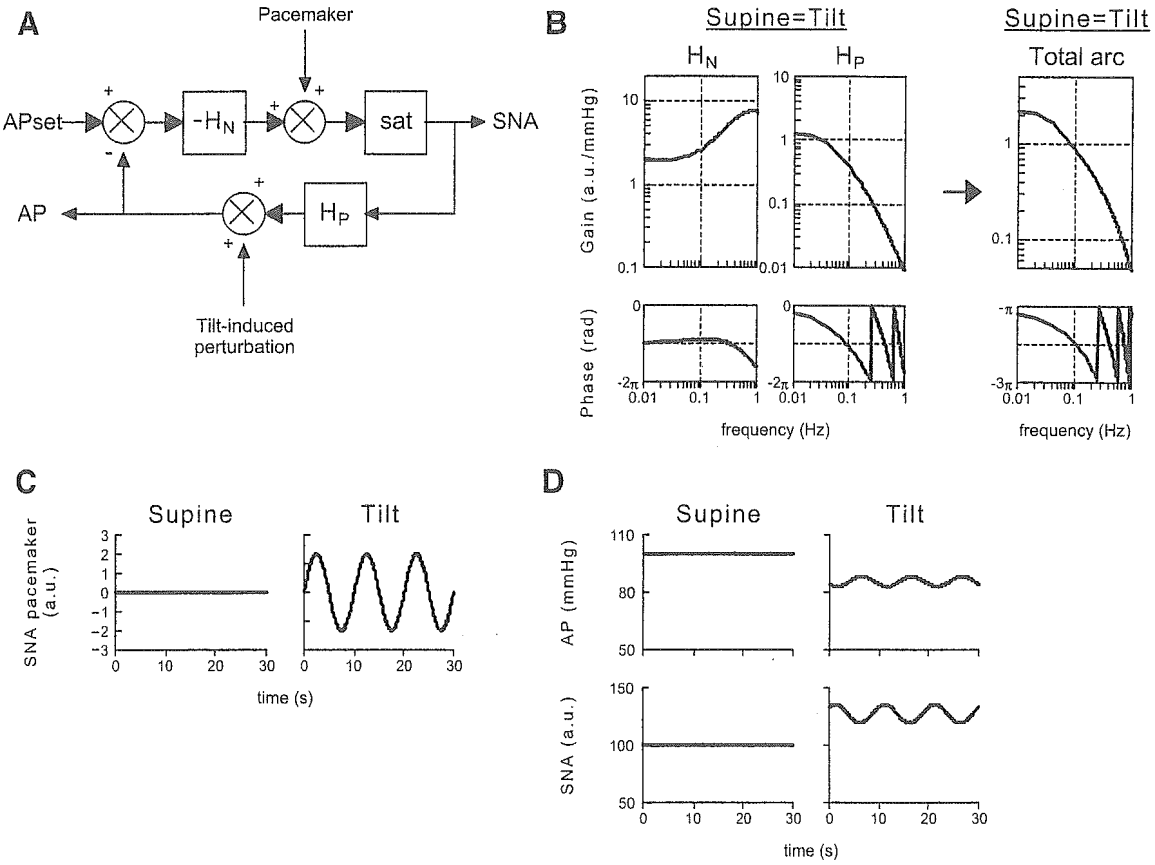

Fig. 8. Simulation of generation of LF oscillation of AP and SNA by the pacemaker oscillator theory. *A*: block diagram of total arc baroreflex system coupled with the SNA pacemaker oscillator. Total arc baroreflex system consists of the neural arc transfer function (H_N), the saturation function (sat), and the neural arc transfer function (H_P). We modeled the SNA pacemaker oscillator as a 0.1-Hz sine wave and assigned tilt-induced perturbation of −50 mmHg in simulations during HUT. We set AP_{set} at 100 mmHg and baseline SNA at 100 AU when AP = AP_{set}. *B*: H_N, H_P, and resultant total arc transfer function (shown as gain and phase). All transfer functions are similar in supine and tilt positions. Because we set K_N = 1.9 AU/mmHg in the model of H_N (see APPENDIX) so that G_0 in total arc is <1 (see Fig. 7), only baroreflex-loop theory cannot generate oscillations of AP and SNA (see Fig. 6). *C*: model of SNA pacemaker oscillator. We set the pacemaker at 0.1-Hz sine wave with amplitude of 2 AU during tilt. Sine wave is absent in supine position. *D*: simulated time series AP and SNA in supine and tilt positions. Increasing amplitude of 0.1-Hz sine wave of the pacemaker oscillator from 0 to 2 AU during tilt generates 0.1-Hz oscillation of AP and SNA.

onset of syncope), AP, MSNA, and their LF oscillations decreased progressively, whereas MSNA remained elevated, during the first stage of development (from 100 to 60 s before onset of syncope). We cannot provide a definitive explanation for the mechanism(s) responsible for this new finding, but we propose the following possibilities.

The first possible explanation is a decrease in neural arc baroreflex transfer gain. A recent finding suggests that the total and neural arc baroreflex gains largely decrease during tilt-induced syncope (19). Our numerical simulation indicates that decreasing H_N gain will attenuate the total arc baroreflex transfer function gain and attenuate G_0 to <1 (Fig. 9*A*). As a result, the baroreflex system could not sustain LF oscillations of AP and SNA (Fig. 9*C*). Although an increase in pure delay of the total baroreflex system theoretically decreases G_0 and suppresses LF oscillations, it might not relate to the decrease in G_0, because our data showed that the frequencies of LF components of AP and MSNA variability were constant during development of tilt-induced syncope. A possible decrease in the baroreflex subsystem transfer gain may also explain the hypotension and sympathetic withdrawal in addition to reductions of LF oscillations (Fig. 9*C*), except withdrawal of MSNA lags behind decreases of AP and LF oscillations of AP and MSNA (from 100 to 60 s before onset of syncope).

The second possible explanation is deactivation of the LF pacemaker oscillator. Our numerical simulation indicates that attenuation of the pacemaker oscillator (Fig. 10*B*) will decrease LF oscillations of AP and SNA (Fig. 10*C*), while the baroreflex system remains constant (Fig. 10*A*). However, the simulation also indicates that the deactivation will not decrease AP and MSNA (Fig. 10*B*). Accordingly, deactivation of the LF pacemaker oscillator does not explain changes in magnitude of AP and MSNA together, whereas the decrease in baroreflex transfer gain explains both decreases.

LF oscillation of MSNA parallels the magnitude of MSNA. Our results may support the concept that LF oscillation of MSNA parallels the magnitude of MSNA. There is increasing evidence that an increase in sympathetic neural firing is accompanied by a proportional enhancement of LF oscillation of MSNA. Consistent with earlier studies (1, 5), we observed that, during early HUT, when AP was well maintained, an increase in MSNA was accompanied by an increase in its LF oscillation. This finding agrees with earlier studies in which stimuli inducing sympathetic activation [nitroprusside administration (20, 24), occlusion of the inferior vena cava (15) and bilateral

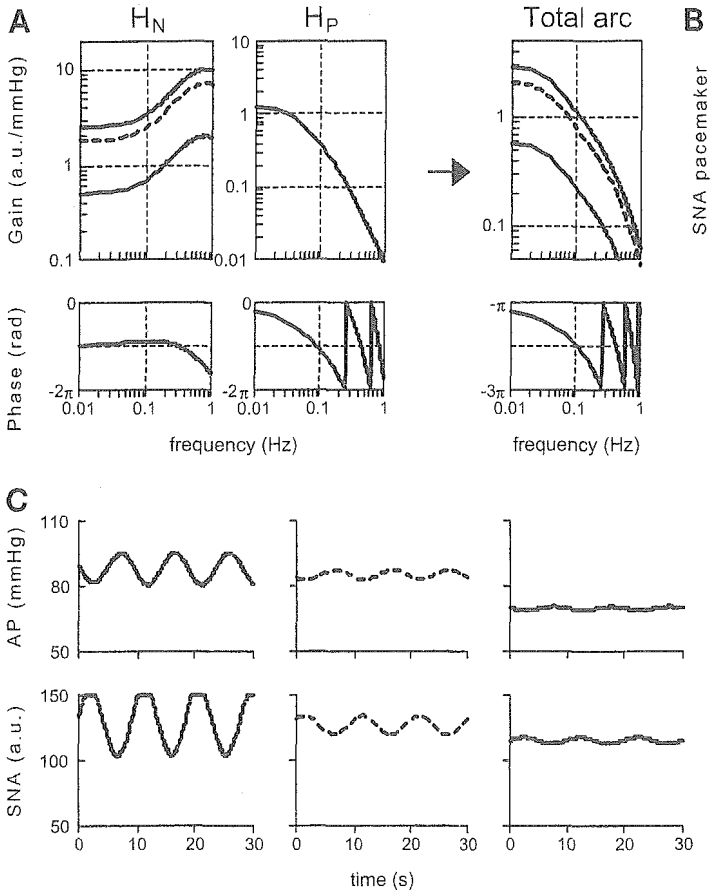

Fig. 9. Simulation of baroreflex impairment during progression of tilt-induced syncope. *A*: H_N, H_P, and resultant total arc transfer function (shown as gain and phase). Static gain of H_N (i.e., K_N) decreases from 2.5 (top solid line) to 1.8 (dashed line) to 0.5 (bottom solid line) AU/mmHg (see APPENDIX). Consequently, G_0 decreases from >1 (top solid line) to <1 (dashed and bottom solid lines). Phase is similar regardless of decrease in gain. *B*: model of SNA pacemaker oscillator. We set the pacemaker at 0.1-Hz sine wave with amplitude of 2 AU throughout tilt. *C*: simulated time series of AP and SNA in supine and tilt positions. *Left*, *middle*, and *right*: simulated data when static gain of H_N was 2.5 (solid line), 1.8 (line), and 0.5 (solid line) AU/mmHg, respectively. We used block diagram of total arc baroreflex system coupled with the SNA pacemaker oscillator in this simulation shown in Fig. 8*A*. We assigned a tilt-induced perturbation of −50 mmHg in simulations during HUT. We set AP_{set} at 100 mmHg and baseline SNA at 100 AU when AP = AP_{set}. Decreasing static gain of H_N attenuates 0.1-Hz oscillation of AP and SNA.

common carotid artery (22), and increase of cerebrospinal fluid pressure (11)] increased LF oscillation of SNA. In addition to demonstrating a link between magnitude of MSNA and LF oscillation of MSNA during sympathetic excitation, our data also suggest that the link may persist even during sympathetic withdrawal in tilt-induced syncope, because we observed that magnitude and LF oscillation of MSNA decreased during HUT-induced syncope.

Respiratory HF component of MSNA variability. As reported earlier (1), the respiratory HF oscillation of MSNA increased during early HUT, when AP was maintained. Several mechanisms may contribute to this increase. *1*) It is likely that downward displacement of the diaphragm reduces inspiratory intrathoracic pressure and inspiratory left ventricular stroke volumes (1, 7). This increases the respiratory HF fluctuation of AP and would increase the respiratory HF oscillation of MSNA via the baroreflex neural arc, in particular, its dynamic high-pass characteristics of H_N (10, 12). If the H_N gain increases during HUT, increases in HF oscillation of MSNA and AP may be further enhanced. *2*) Because early HUT decreases the respiratory HF fluctuation of the R-R interval, which is known to decrease the respiratory HF fluctuation of AP (25), it would increase the HF fluctuation of AP (1). *3*) Because HUT induces hyperpnea during normotensive HUT (13), the respiratory-related oscillation of MSNA might be increased. Unfortunately, because numerical data are not available for the transfer characteristics involved in these possible explanations, we cannot simulate how these possibilities generate the respiratory HF oscillations.

This study investigated respiratory HF oscillation of MSNA during tilt-induced syncope. We found that HF oscillation of MSNA decreased just before onset of tilt-induced syncope. We cannot determine the mechanism(s) for this observation but propose the following explanations. The first possibility is that the baroreflex neural arc gain decreases during the progression of tilt-induced syncope, resulting in a decrease of the respiratory HF oscillation of MSNA. This can explain our finding that HF oscillation of MSNA decreased whereas HF oscillation of AP remained elevated during tilt-induced syncope, because the peripheral arc low-pass filter characteristics (12) would limit the reduction of HF oscillation of AP and keep HF oscillation of AP elevated. The second possibility is that tidal volume decreases during development of tilt-induced syncope. When tidal volume decreases, the lung will be less inflated. Consequently, MSNA will be less suppressed by lung inflation, reducing respiratory modulation of MSNA.

Our results indicate a decrease in MSNA and an increase in cardiac vagal nerve activity in development of tilt-induced syncope. In contrast to HF amplitude of MSNA variability, HF amplitude of R-R interval variability increased markedly just before onset of orthostatic syncope, consistent with earlier reports (4). This finding indicates an excitation of cardiac vagal outflow to the heart. In addition, LF amplitude of R-R interval variability also increased just before onset of syncope, in agreement with a previous study (13). This might also be explained by excitation of vagal, but not sympathetic, nerve activity, because MSNA and heart rate decrease in this stage.

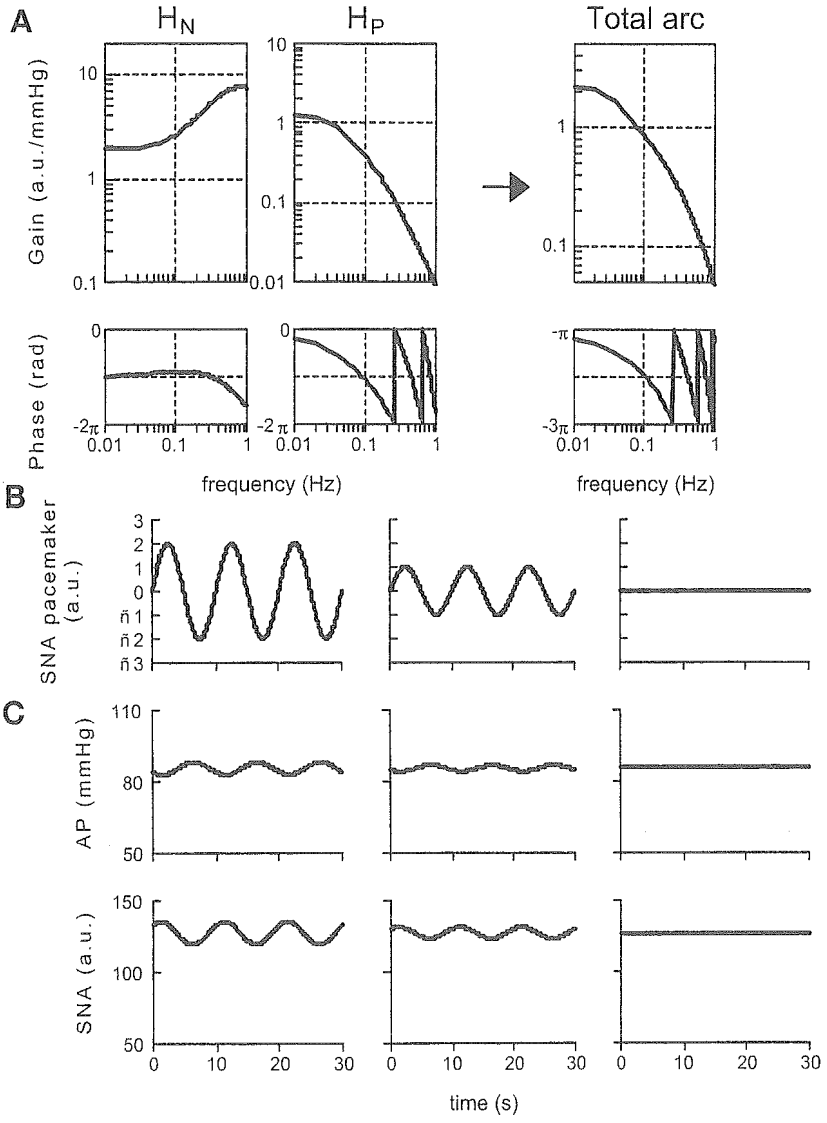

Fig. 10. Simulation of pacemaker oscillator attenuation during progression of tilt-induced syncope. *A*: H_N, H_P, and resultant total arc transfer function (shown as gain and phase) are constant. Static gain of H_N (i.e., K_N) was set at 1.9 AU/mmHg (see APPENDIX), and, as a result, $G_0 < 1$. *B*: model of SNA pacemaker oscillator. We set pacemaker at 0.1-Hz sine wave with amplitudes of 2, 1, and 0 AU (*left, middle*, and *right*, respectively). *C*: simulated time series of AP and SNA in supine and tilt positions. *Left, middle*, and *right*: simulated data when pacemaker oscillator was set as shown in *left, middle*, and *right* of *B*. We used the block diagram of total arc baroreflex system coupled with SNA pacemaker oscillator in this simulation, as shown in Fig. 8*A*. We assigned tilt-induced perturbation of −50 mmHg in simulations during HUT. We set AP_{set} at 100 mmHg and baseline SNA at 100 AU when AP = AP_{set}. Decreasing amplitude of the 0.1-Hz sine wave of the pacemaker oscillator from 2 (*left*) to 1 (*middle*) to 0 (*right*) AU progressively decreases the 0.1-Hz oscillation of AP and SNA.

Limitations. This study has several limitations. *1*) We studied healthy subjects with no recent history of spontaneous syncope. Therefore, it is difficult to generalize our findings to patients with recurrent and chronic orthostatic hypotension (3, 17, 18). *2*) We did not measure tidal volume, arterial P_{CO_2}, and pH, which may affect MSNA and AP and their fluctuations. *3*) We measured AP wave changes during HUT by noninvasive photoplethysmography. Nevertheless, the photoplethysmographic pressure waveform correlated very well with invasive intra-arterial pressure during tilt (21). *4*) Because the baroreflex transfer functions of total, neural, and peripheral arcs have not been determined in humans, we used the characteristics of transfer function derived from animal studies (rabbits) (10, 12) in numerical simulations of AP, MSNA, and their oscillations. *5*) Our model used in the numerical simulation focused on baroreflex-loop and pacemaker theories governing SNA and did not incorporate vagal nerve activity into the model.

In conclusion, LF oscillation of MSNA decreases at the initial development of orthostatic neurally mediated syncope, before sympathetic withdrawal, bradycardia, and severe hypotension, to the level of syncope.

APPENDIX

In rabbits, the transfer function of the baroreflex neural arc (baroreceptor pressure to SNA) approximates derivative characteristics of frequencies <0.8 Hz and high-cut characteristics of frequencies >0.8 Hz (12). Therefore, according to our previous study, we model the neural arc transfer function (H_N) as follows

$$H_N(f) = -K_N \frac{1 + \frac{f}{f_{c1}}j}{\left(1 + \frac{f}{f_{c2}}\right)^2} \exp(-2\pi f j L) \qquad (A1)$$

where f and j represent frequency (in Hz) and imaginary units, respectively; K_N is static gain (in AU/mmHg), f_{c1} and f_{c2} ($f_{c1} < f_{c2}$) are corner frequencies (in Hz) for derivative and high-cut characteristics, respectively, and L is a pure delay (in s), which would represent the sum of delays in the synaptic transmission at the baroreflex central pathways and the sympathetic ganglion. The dynamic gain increases from f_{c1} to f_{c2} and decreases above f_{c2}. We set f_{c1}, f_{c2}, and L at 0.1, 0.8, and 0.2, respectively, in all simulations in Figs. 6, 8, 9, and 10. We set K_N appropriately in each simulation (Figs. 6, 8, 9, and 10).

In addition, the transfer function of the baroreflex peripheral arc (SNA to systemic AP) approximates the second-order low-pass filter with a lag time in rabbits (12). Therefore, we model the peripheral arc transfer function (H_P) as follows

$$H_P(f)=\frac{K_P}{1+2\zeta\frac{f}{f_N}j+\left(\frac{f}{f_N}j\right)^2}\exp(-2\pi fjL) \qquad (A2)$$

where K_P is static gain (in mmHg/AU), f_N and ζ represent natural frequency (in Hz) and damping ratio, respectively, and L is a pure delay (in s), which would represent the sum of delays in the synaptic transmission at the neuroeffector junction and the intracellular signal transduction in the effector organs. We set K_P, f_N, ζ, and L at 1.3, 0.07, 1.4 and 2.4, respectively, in all simulations in Figs. 6, 8, 9, and 10 by modifying these parameter values observed in rabbits (12) to simulate AP oscillation at ~0.1 Hz in humans.

Consequently, the transfer function of the total arc baroreflex system (baroreceptor pressure to systemic AP) in our model (Fig. 6*A*) approximates the first-order low-pass filter with a pure delay (10) as follows

$$H(f)=\frac{K_T}{1+\frac{f}{f_c}j}\exp(-2\pi fjL) \qquad (A3)$$

where K_T is static gain (in mmHg/mmHg), f_c is corner frequency (in Hz), and L is pure delay (in s) of the total arc system. The "sat" function in Figs. 6*A* and 8*A* is a saturation function that determines minimum (−50 AU) and maximum SNA (50 AU).

GRANTS

This study was supported by New Energy and Industrial Technology Development Organization of Japan Industrial Technology Research Grant Program 03A47075.

REFERENCES

1. **Cooke WH, Hoag JB, Crossman AA, Kuusela TA, Tahvanainen KU, and Eckberg DL.** Human responses to upright tilt: a window on central autonomic integration. *J Physiol* 517: 617–628, 1999.
2. **DeBoer RW, Karemaker JM, and Strackee J.** Hemodynamic fluctuations and baroreflex sensitivity in humans: a beat-to-beat model. *Am J Physiol Heart Circ Physiol* 253: H680–H689, 1987.
3. **Furlan R, Jacob G, Snell M, Robertson D, Porta A, Harris P, and Mosqueda-Garcia R.** Chronic orthostatic intolerance: a disorder with discordant cardiac and vascular sympathetic control. *Circulation* 98: 2154–2159, 1998.
4. **Furlan R, Piazza S, Dell'Orto S, Barbic F, Bianchi A, Mainardi L, Cerutti S, Pagani M, and Malliani A.** Cardiac autonomic patterns preceding occasional vasovagal reactions in healthy humans. *Circulation* 98: 1756–1761, 1998.
5. **Furlan R, Porta A, Costa F, Tank J, Baker L, Schiavi R, Robertson D, Malliani A, and Mosqueda-Garcia R.** Oscillatory patterns in sympathetic neural discharge and cardiovascular variables during orthostatic stimulus. *Circulation* 101: 886–892, 2000.
6. **Guyton A and Harris J.** Pressoreceptor-autonomic oscillation: a probable cause of vasomotor waves. *Am J Physiol* 165: 158–166, 1951.
7. **Guz A, Innes JA, and Murphy K.** Respiratory modulation of left ventricular stroke volume in man measured using pulsed Doppler ultrasound. *J Physiol* 393: 499–512, 1987.
8. **Hayano J, Mukai S, Fukuta H, Sakata S, Ohte N, and Kimura G.** Postural response of low-frequency component of heart rate variability is an increased risk for mortality in patients with coronary artery disease. *Chest* 120: 1942–1952, 2001.
9. **Hayano J, Taylor JA, Yamada A, Mukai S, Hori R, Asakawa T, Yokoyama K, Watanabe Y, Takata K, and Fujinami T.** Continuous assessment of hemodynamic control by complex demodulation of cardiovascular variability. *Am J Physiol Heart Circ Physiol* 264: H1229–H1238, 1993.
10. **Ikeda Y, Kawada T, Sugimachi M, Kawaguchi O, Shishido T, Sato T, Miyano H, Matsuura W, Alexander J Jr, and Sunagawa K.** Neural arc of baroreflex optimizes dynamic pressure regulation in achieving both stability and quickness. *Am J Physiol Heart Circ Physiol* 271: H882–H890, 1996.
11. **Kaminsky R, Meyer G, and Winter D.** Sympathetic unit activity associated with Mayer waves in the spinal dog. *Am J Physiol* 219: 1768–1771, 1970.
12. **Kawada T, Zheng C, Yanagiya Y, Uemura K, Miyamoto T, Inagaki M, Shishido T, Sugimachi M, and Sunagawa K.** High-cut characteristics of the baroreflex neural arc preserve baroreflex gain against pulsatile pressure. *Am J Physiol Heart Circ Physiol* 282: H1149–H1156, 2002.
13. **Lipsitz LA, Hayano J, Sakata S, Okada A, and Morin RJ.** Complex demodulation of cardiorespiratory dynamics preceding vasovagal syncope. *Circulation* 98: 977–983, 1998.
14. **Mano T.** Microneurography as a tool to investigate sympathetic nerve responses to environmental stress. *Aviakosm Ekolog Med* 31: 8–14, 1997.
15. **Montano N, Lombardi F, Gnecchi Ruscone T, Contini M, Finocchiaro ML, Baselli G, Porta A, Cerutti S, and Malliani A.** Spectral analysis of sympathetic discharge, R-R interval and systolic arterial pressure in decerebrate cats. *J Auton Nerv Syst* 40: 21–31, 1992.
16. **Morillo CA, Eckberg DL, Ellenbogen KA, Beightol LA, Hoag JB, Tahvanainen KU, Kuusela TA, and Diedrich AM.** Vagal and sympathetic mechanisms in patients with orthostatic vasovagal syncope. *Circulation* 96: 2509–2513, 1997.
17. **Mosqueda-Garcia R, Furlan R, Fernandez-Violante R, Desai T, Snell M, Jarai Z, Ananthram V, Robertson RM, and Robertson D.** Sympathetic and baroreceptor reflex function in neurally mediated syncope evoked by tilt. *J Clin Invest* 99: 2736–2744, 1997.
18. **Mosqueda-Garcia R, Furlan R, Tank J, and Fernandez-Violante R.** The elusive pathophysiology of neurally mediated syncope. *Circulation* 102: 2898–2906, 2000.
19. **Ogoh S, Volianitis S, Raven PB, and Secher NH.** Carotid baroreflex function ceases during vasovagal syncope. *Clin Auton Res* 14: 30–33, 2004.
20. **Pagani M, Montano N, Porta A, Malliani A, Abboud FM, Birkett C, and Somers VK.** Relationship between spectral components of cardiovascular variabilities and direct measures of muscle sympathetic nerve activity in humans. *Circulation* 95: 1441–1448, 1997.
21. **Petersen ME, Williams TR, and Sutton R.** A comparison of non-invasive continuous finger blood pressure measurement (Finapres) with intra-arterial pressure during prolonged head-up tilt. *Eur Heart J* 16: 1641–1654, 1995.
22. **Preiss G and Polosa C.** Patterns of sympathetic neuron activity associated with Mayer waves. *Am J Physiol* 226: 724–730, 1974.
23. **Rowell LB.** *Human Cardiovascular Control.* New York: Oxford University Press, 1993.
24. **Saul JP, Rea RF, Eckberg DL, Berger RD, and Cohen RJ.** Heart rate and muscle sympathetic nerve variability during reflex changes of autonomic activity. *Am J Physiol Heart Circ Physiol* 258: H713–H721, 1990.
25. **Taylor JA and Eckberg DL.** Fundamental relations between short-term RR interval and arterial pressure oscillations in humans. *Circulation* 93: 1527–1532, 1996.

Am J Physiol Heart Circ Physiol 289: H1604–H1609, 2005.
First published May 20, 2005; doi:10.1152/ajpheart.00053.2005.

Static interaction between muscle mechanoreflex and arterial baroreflex in determining efferent sympathetic nerve activity

Kenta Yamamoto,[1,2] Toru Kawada,[1] Atsunori Kamiya,[1] Hiroshi Takaki,[1] Masaru Sugimachi,[1] and Kenji Sunagawa[3]

[1]*Department of Cardiovascular Dynamics, National Cardiovascular Center Research Institute, Osaka;* [2]*Pharmaceuticals and Medical Devices Agency, Tokyo; and* [3]*Department of Cardiovascular Medicine, Graduate School of Medical Sciences, Kyushu University, Fukuoka, Japan*

Submitted 18 January 2005; accepted in final form 13 May 2005

Yamamoto, Kenta, Toru Kawada, Atsunori Kamiya, Hiroshi Takaki, Masaru Sugimachi, and Kenji Sunagawa. Static interaction between muscle mechanoreflex and arterial baroreflex in determining efferent sympathetic nerve activity. *Am J Physiol Heart Circ Physiol* 289: H1604–H1609, 2005. First published May 20, 2005; doi:10.1152/ajpheart.00053.2005.—Elucidation of the interaction between the muscle mechanoreflex and the arterial baroreflex is essential for better understanding of sympathetic regulation during exercise. We characterized the effects of these two reflexes on sympathetic nerve activity (SNA) in anesthetized rabbits ($n = 7$). Under open-loop baroreflex conditions, we recorded renal SNA at carotid sinus pressure (CSP) of 40, 80, 120, or 160 mmHg while passively stretching the hindlimb muscle at muscle tension (MT) of 0, 2, 4, or 6 kg. The MT-SNA relationship at CSP of 40 mmHg approximated a straight line. Increase in CSP from 40 to 120 and 160 mmHg shifted the MT-SNA relationship downward and reduced the response range (the difference between maximum and minimum SNA) to 43 ± 10% and 19 ± 6%, respectively ($P < 0.01$). The CSP-SNA relationship at MT of 0 kg approximated a sigmoid curve. Increase in MT from 0 to 2, 4, and 6 kg shifted the CSP-SNA relationship upward and extended the response range to 133 ± 8%, 156 ± 14%, and 178 ± 15%, respectively ($P < 0.01$). A model of algebraic summation, i.e., parallel shift, with a threshold of SNA functionally reproduced the interaction of the two reflexes ($y = 1.00x - 0.01$; $r^2 = 0.991$, root mean square = 2.6% between estimated and measured SNA). In conclusion, the response ranges of SNA to baroreceptor and muscle mechanoreceptor input changed in a manner that could be explained by a parallel shift with threshold.

muscle stretch; exercise pressor reflex; exercise; subliminal fringe

ARTERIAL PRESSURE (AP) during exercise is regulated by neural inputs from three principal sources (19): efferent inputs from supramedullary regions, known as the central command; afferent inputs from contraction-sensitive skeletal muscle receptors, known as the exercise pressor reflex; and afferent inputs from baroreceptor populations such as the arterial and cardiopulmonary baroreflexes. Elucidation of the interaction among these inputs is essential for understanding the AP regulation during exercise, and it has been extensively studied (2–6, 11, 14–18, 22, 26). We previously demonstrated (26) that activation of muscle mechanoreceptors (muscle mechanoreflex) resets the arterial baroreflex control of sympathetic nerve activity (SNA), possibly compensating for a reduction in AP resulting from exercise-induced vasodilation. However, how these reflexes quantitatively interact with each other in regulating SNA over a wide range of inputs remains unknown.

Recent studies (13, 26) demonstrated that treadmill exercise or the muscle mechanoreflex extends the response range of SNA (i.e., the difference between maximum and minimum SNA) in the arterial baroreflex. The extension of the response range was mainly attributed to an increase in maximum SNA but not to changes in minimum SNA. On the other hand, Potts and Li (16) showed that higher carotid sinus pressure (CSP) attenuates the pressor response induced by the muscle mechanoreflex compared with lower CSP. We therefore hypothesized that the response range of SNA to either the muscle mechanoreflex or the arterial baroreflex would be changed depending on the afferent inputs from the other reflex.

To test the above-described hypothesis, we examined the static SNA responses to a combination of a wide range of inputs (4 different levels of baroreceptor input and 4 different levels of muscle mechanoreceptor input) in anesthetized rabbits. The results indicated that the response ranges of SNA to baroreceptor and muscle mechanoreceptor input can change depending on the input from the other reflex.

MATERIALS AND METHODS

Surgical preparations. Animals were cared for in strict accordance with the "Guiding Principles for the Care and Use of Animals in the Field of Physiological Sciences" approved by the Physiological Society of Japan. All protocols were approved by the Animal Subjects Committee of the National Cardiovascular Center. Seven Japanese White rabbits weighing 2.6–3.0 kg were anesthetized via intravenous injection (2 ml/kg) of a mixture of urethane (250 mg/ml) and α-chloralose (40 mg/ml) and were mechanically ventilated with oxygen-enriched room air. Supplemental anesthetics (0.2–0.3 $ml \cdot kg^{-1} \cdot h^{-1}$) were administered continuously to maintain stable AP and heart rate levels during intervals of experimental protocols, which were indicative of an appropriate level of anesthesia. Arterial blood was sampled from the left common carotid artery. The rabbits were slightly hyperventilated to suppress chemoreflexes (arterial P_{CO_2} ranged from 30 to 35 mmHg, arterial $P_{O_2} > 300$ mmHg). Arterial blood pH was within the physiological range when examined at the end of surgical preparation, as well as at the end of the experiment. The body temperature of each animal was maintained at ~38°C with a heating pad. AP was measured with a high-fidelity pressure transducer (Millar Instruments, Houston, TX) inserted from the right femoral artery.

We isolated bilateral carotid sinuses from the systemic circulation by ligating the internal and external carotid arteries and other small branches originating from the carotid sinus region. The isolated

Address for reprint requests and other correspondence: K. Yamamoto, Dept. of Cardiovascular Dynamics, National Cardiovascular Center Research Institute, 5-7-1 Fujishirodai, Suita, Osaka 565-8565, Japan (e-mail: kentay@ri.ncvc.go.jp).

The costs of publication of this article were defrayed in part by the payment of page charges. The article must therefore be hereby marked "*advertisement*" in accordance with 18 U.S.C. Section 1734 solely to indicate this fact.

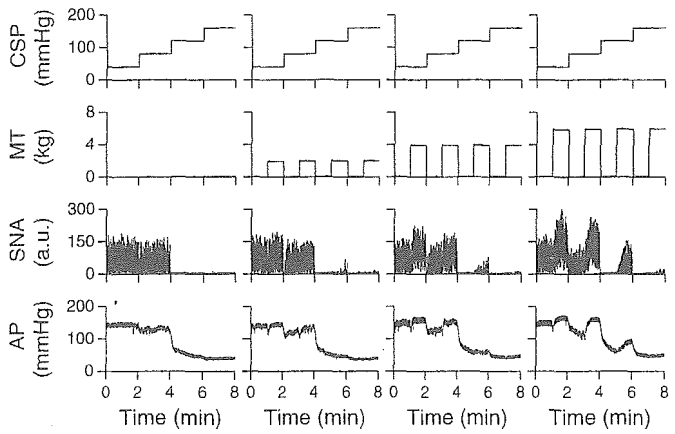

Fig. 1. Typical time series of intracarotid sinus pressure (CSP), muscle tension (MT), sympathetic nerve activity [SNA; in arbitrary units (a.u.)], and arterial pressure (AP) obtained from 1 animal. The 4 panels correspond to MT of 0, 2, 4, and 6 kg, in that order. SNA and AP decreased in response to increments in CSP at all MT levels. SNA and AP increased in response to the increments in MT at CSP below 120 mmHg in this animal. Data were resampled at 10 Hz.

carotid sinuses were filled with warmed physiological saline via catheters inserted through the common carotid arteries. CSP was controlled by a servo-controlled piston pump (model ET-126A, Labworks, Costa Mesa, CA). Bilateral vagal and aortic depressor nerves were sectioned at the neck to minimize reflexes from the cardiopulmonary region and from the aortic arch.

We exposed the left renal sympathetic nerve retroperitoneally and attached a pair of stainless steel wire electrodes (Bioflex wire AS633, Cooner Wire) to record SNA. The nerve bundle peripheral to the electrodes was tightly ligated and crushed to eliminate afferent signals from the kidney. The nerve and electrodes were secured with silicone glue (Kwik-Sil, World Precision Instruments, Sarasota, FL). The preamplified nerve signal was band-pass filtered at 150–1,000 Hz, full-wave rectified, and low-pass filtered with a cutoff frequency of 30 Hz to quantify the nerve activity. Pancuronium bromide (0.1 mg/kg) was administered to prevent muscular activity from contaminating the SNA recordings.

With the rabbit in the prone position, the sacrum, left ankle, and knee were clamped with a custom-made apparatus to prevent body trunk and hindlimb movement during muscle stretch. The left triceps surae muscle, Achilles tendon, and calcaneus bone were exposed. The left triceps surae muscle was isolated from surrounding tissue. The Achilles tendon was severed from the calcaneus bone and attached to a force transducer (Load Cell LUR-A-SA1, Kyowa Electronic Instruments, Tokyo, Japan). During muscle stretch, the other side of the force transducer was connected to a weight via a pulley; muscle tension (MT) was quantified with this force transducer.

Protocols. We measured the steady-state SNA response to a number of combinations of CSP and MT as follows. CSP was initially decreased to 40 mmHg. After attainment of a steady state, CSP was increased from 40 to 160 mmHg in increments of 40 mmHg. Each pressure step was maintained for 120 s. Passive muscle stretch was applied during the last 60 s of each CSP step to develop MT. We repeated the stepwise CSP input four times while varying MT by 0, 2, 4, and 6 kg in random orders.

Data analysis. We recorded CSP, MT, SNA, and AP at a sampling rate of 200 Hz with a 12-bit analog-to-digital converter. Data were stored on a dedicated laboratory computer system for later analyses.

We calculated mean SNA and AP during the last 10 s of each CSP step. Because the absolute magnitude of SNA depended on recording conditions, SNA was presented in arbitrary units (a.u.) so that the minimum and maximum values of SNA data during the stepwise CSP input under 0-kg MT became 0 and 100 a.u., respectively, for each animal. We calculated the response range of SNA (the difference between maximum and minimum SNA) to the carotid sinus baroreflex based on the CSP-SNA relationship obtained at each MT level. We also calculated the response range of SNA to the muscle mechanoreflex based on the MT-SNA relationship obtained at each CSP level.

Statistical analysis. All data are presented as means ± SE. Differences were considered significant when $P < 0.05$. The effects of CSP and MT on SNA were tested by two-way ANOVA with repeated measurements. The response range of SNA in the CSP-SNA relationship or in the MT-SNA relationship was compared by one-way ANOVA with repeated measurements. In the case of a significant F-value, a post hoc test with the Newman-Keuls method was used to identify significant differences between any two of the conditions.

RESULTS

Figure 1 shows a typical time series of CSP, MT, SNA, and AP obtained from one animal. Although the panels are arranged in Fig. 1 in increasing order of MT, the MT levels were applied randomly in the experiments. SNA and AP decreased in response to the increments in CSP with all MT levels. SNA and AP increased in response to the increments in MT at CSP below 120 mmHg in this animal.

Figure 2*A* illustrates the mean MT-SNA relationship at each CSP level. SNA proportionally increased in response to the increments in MT at CSP of 40 and 80 mmHg. However, SNA did not increase at CSP of 120 mmHg, except at MT of 6 kg. Furthermore, the level of MT did not affect SNA at CSP of 160 mmHg.

Figure 2*B* illustrates the mean CSP-SNA relationship at each MT level. SNA decreased in response to increments in CSP with all MT levels. The CSP-SNA relationship approximated a sigmoid curve and was shifted upward with increasing MT. The increase in MT extended the response range of SNA to the carotid sinus baroreflex.

Two-way ANOVA indicated a significant interaction between MT and CSP in determining SNA ($P < 0.001$), suggest-

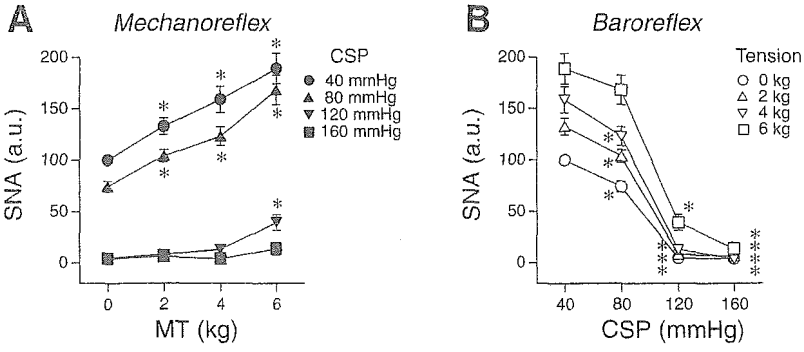

Fig. 2. Muscle mechanoreflex at each CSP level (*A*) and carotid sinus baroreflex at each MT level (*B*). In the MT-SNA relationship (*A*), SNA proportionally increased in response to increments in MT at CSP of 40 and 80 mmHg. However, SNA did not increase except at MT of 6 kg at CSP of 120 mmHg and did not change at any MT level at CSP of 160 mmHg. In the CSP-SNA relationship (*B*), SNA decreased in response to increments in CSP at all MT levels. Two-way ANOVA indicated that there was a significant interaction between CSP and MT in determining SNA ($P < 0.001$). *$P < 0.05$ compared with MT of 0 kg at each CSP in the muscle mechanoreflex (*A*) and compared with CSP of 40 mmHg at each MT in the carotid sinus baroreflex (*B*).

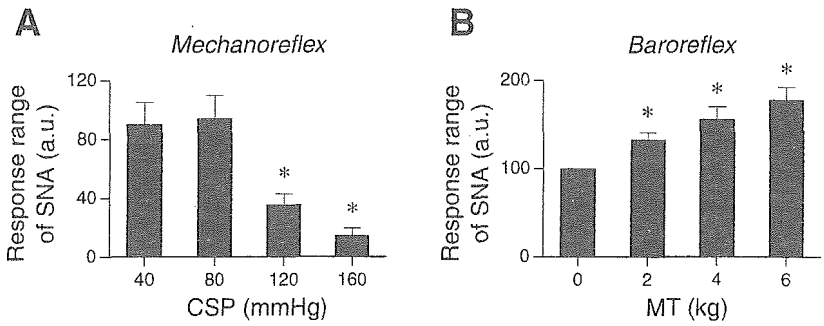

Fig. 3. Response range of SNA to the muscle mechanoreflex (*A*) and to the carotid sinus baroreflex (*B*). The response range to the muscle mechanoreflex (*A*) was smaller at CSP of 120 and 160 mmHg than at CSP of 40 mmHg. The response range to the carotid sinus baroreflex (*B*) was greater at MT of 2, 4, and 6 kg than at MT of 0 kg. $*P < 0.05$ compared with CSP of 40 mmHg in the muscle mechanoreflex (*A*) and compared with MT of 0 kg in the carotid sinus baroreflex (*B*).

ing that the effects of the muscle mechanoreflex and the arterial baroreflex could not be explained by algebraic summation (15, 16).

The response range of SNA to the muscle mechanoreflex obtained at each CSP level is shown in Fig. 3*A*. The response range of SNA was significantly smaller at CSP of 120 and 160 mmHg than at CSP of 40 mmHg.

The response range of SNA to the carotid sinus baroreflex obtained at each MT level is shown in Fig. 3*B*. The response range of SNA was significantly greater at MT of 2, 4, and 6 kg than at 0 kg.

Figure 4 illustrates the relationship between SNA and AP obtained by 16 combinations of 4 levels of CSP and 4 levels of MT. The relationship between SNA and AP can be characterized by a single sigmoid curve, indicating that the relationship between SNA and AP does not differ between the muscle mechanoreflex and the carotid sinus baroreflex.

DISCUSSION

The key findings of the present study were as follows. First, an increase in CSP from 40 to 80 mmHg caused a parallel downward shift in the MT-SNA relationship, and a further increase in CSP reduced the response range of SNA for the muscle mechanoreflex. Secondly, an increase in MT shifted the CSP-SNA relationship upward, extending the response range of SNA for the carotid sinus baroreflex. These results suggest that the response ranges of SNA to baroreceptor and muscle

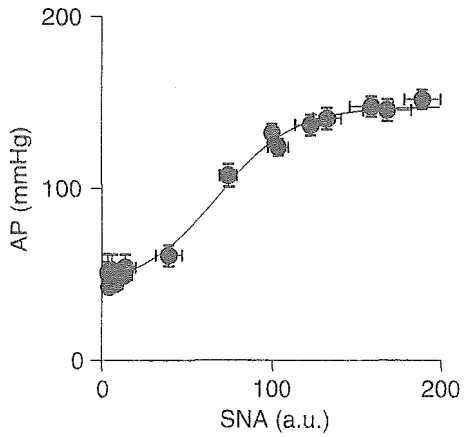

Fig. 4. Relationship between SNA and AP obtained by 16 combinations of 4 levels of CSP and 4 levels of MT. The relationship between SNA and AP can be characterized by a single sigmoid curve, indicating that the SNA-AP relationship did not differ between the muscle mechanoreflex and the carotid sinus baroreflex.

mechanoreceptor inputs can change depending on the input from the other reflex.

Interaction between muscle mechanoreflex and arterial baroreflex. We determined the maximum MT based on a preliminary study in which the SNA response to MT did not saturate at 6 kg. The accurate range for MT to mimic the physiological activation of muscle mechanoreceptor afferents was unclear. The maximum MT in the present study was threefold as strong as that which could occur if the configuration of Achilles tendon and calcaneus bone was kept intact (23). Although the maximum MT of 6 kg was nonphysiological and might have recruited nociceptive or nonspecific fiber activation, the SNA increased linearly with MT at CSP of 40 and 80 mmHg (Fig. 2*A*). Accordingly, the transition of physiological nonnociceptive stimulation to nonphysiological nociceptive stimulation was not clearly determined in the present experimental settings. The muscle mechanoreflex is mediated by group III and IV afferents (10, 12). The proportion of contraction-sensitive units with presumably mechanical mechanism of activation is higher among group III than group IV afferents (7). Discharge of group IV afferents is enhanced when the muscle is made ischemic. The dominant fiber type might have changed when the stimulation changed from nonnociceptive to nociceptive. Another concern is that because nociceptive stimulation of muscle afferents by metabolic products of contraction is likely to be related to exercise but stimulation by nonphysiological levels of stretch is not, the physiological significance of the present results should be interpreted carefully.

The effect of baroreceptor input on muscle mechanoreflex control of SNA has never been analyzed quantitatively over a wide range of inputs. SNA proportionally increased in response to increments in MT at CSP of 40 and 80 mmHg (Fig. 2*A*). However, SNA did not increase at CSP of 120 mmHg until MT of 6 kg was applied (Fig. 2*A*). As a result, the response range of SNA to MT was reduced by an increase in CSP (Fig. 3*A*). These data suggest that greater tension development above a certain level is necessary to evoke sympathoexcitation by the muscle mechanoreflex at higher CSP. Stebbins et al. (23) demonstrated that mean AP increased with increasing passive muscle stretch up to 8 kg, which suggests the SNA increase during passive muscle stretch. However, the AP response to passive muscle stretch might be modified by the accompanying arterial baroreflex in their study, because they did not open the arterial baroreflex negative-feedback loop. Potts and Li (16) demonstrated that higher CSP attenuated the sympathoexcitatory responses induced by muscle mechanoreflex. The present study extended the results by Potts

and Li (16) by directly measuring SNA over a wide range of mechanoreceptor and baroreceptor inputs.

Elevation of MT increased the response range of SNA to CSP to ~130%, 160%, and 180% at MT of 2, 4, and 6 kg, respectively, relative to that observed under MT of 0 kg (Fig. 3*B*). These results are consistent with results by Miki et al. (13), who demonstrated that treadmill exercise increases the response range of SNA in the arterial baroreflex. Muscle mechanoreflex may contribute to the extended response range of SNA in the arterial baroreflex during exercise. The pressor response was observed during tetanic contraction of the hindlimb induced by femoral nerve stimulation at 100 Hz in anesthetized and baroreceptor-deafferentiated rabbits (24). The static contraction also induces the pressor response in decerebrated rabbits (25). However, rhythmic contraction of the hindlimb by 3-Hz stimulation of the femoral nerve decreases mean AP (24). Both pressor and depressor responses were initiated from the contracting limbs, as both responses were eliminated after sectioning of the somatic nerves. To what extent the opposing reflexes participate in the regulation of SNA and AP during exercise awaits further investigation.

Our data are the first to demonstrate that sympathoexcitation induced by the muscle mechanoreflex requires development of a strong tension when CSP is high. On the other hand, weak tension development is sufficient to evoke sympathoexcitation at a lower CSP, possibly antagonizing a further reduction in AP during exercise (1, 16). An increased response range of SNA to CSP by muscle mechanoreceptor activation may also improve the pressure-stabilizing capacity of the arterial baroreflex against larger pressure disturbances such as those occurring during exercise (26). Furthermore, the muscle mechanoreflex and the carotid sinus baroreflex share a common output variable of SNA with regard to the regulation of AP, because the SNA-AP relationship cannot be discriminated between MT and CSP perturbations (Fig. 4). Together, these findings suggest that interaction of the two reflexes is beneficial to compensate for AP decreases resulting from exercise-induced vasodilation while maintaining the stabilization of AP against pressure disturbances.

Functional model for interaction between muscle mechanoreflex and carotid sinus baroreflex. A functional model of a given system is useful for understanding the physiological system through a simulation study. One can examine the performance of a given physiological system by simulating what would happen if the parameters of the model deviated from their normal physiological values. For instance, we have reported (8) the importance of high-cut baroreflex neural arc transfer characteristics in AP regulation by removing the high-cut characteristics in the simulation. Another application of a functional model is that it can provide a basis for development of an artificial device to support or replace the impaired physiological system. For instance, we have identified dynamic characteristics of the arterial baroreflex system and developed a framework of an artificial baroreflex center that can replace the failed vasomotor center (20, 21, 27). Currently, the artificial baroreflex center does not take account of any interactions from afferent inputs other than the baroreceptors. Quantitative analysis of interaction between the mechanoreflex and the arterial baroreflex is the first step toward the future improvement of the artificial baroreflex center, when the artificial baroreflex center will be able to adjust its function during exercise.

We constructed a functional model to reproduce the interaction between the muscle mechanoreflex and the carotid sinus baroreflex. The CSP-SNA relationship has been modeled by a sigmoid curve as follows (9):

$$SNA_B(CSP) = \frac{P_1}{1 + \exp[P_2(CSP - P_3)]} + P_4 \qquad (1)$$

where SNA_B is SNA derived from the baroreflex, P_1 denotes the response range (i.e., the difference between the maximum and minimum values of SNA), P_2 is the coefficient of gain, P_3 is the midpoint of the logistic function on the CSP axis, and P_4 is the minimum value of SNA.

The MT-SNA relationship can be modeled by a linear function as follows:

$$SNA_M(MT) = A_1 \cdot MT + A_2 \qquad (2)$$

where SNA_M is SNA derived from the mechanoreflex, and A_1 and A_2 represent the slope and intercept, respectively. The linear model was based on the MT-SNA relationship at CSP of 40 and 80 mmHg (Fig. 2*A*).

We then constructed an integrative model from the above two models. We first constructed an algebraic summation model based on the MT-SNA relationship, which showed a parallel shift between CSP of 40 and 80 mmHg. To remove apparent changes in parameters in *Eq. 1* for different MT and nonlinearity observed in the MT-SNA relationship for higher CSP, we introduced threshold in the summation model as follows:

$$SNA(CSP, MT) = \max[SNA_B(CSP) + SNA_M(MT), Th] \qquad (3)$$

where Th is a threshold value for SNA. The function $\max(a, b)$ gives the greater or equal value between a and b.

Figure 5 illustrates a hypothetical interaction between the muscle mechanoreflex and the arterial baroreflex in a model of algebraic summation with threshold (*Eq. 3*). Figure 5*A* is a simplified block diagram of the functional integration of two reflexes. The SNA control signals derived from the muscle mechanoreflex and the arterial baroreflex are summed, and then SNA is evoked if the sum exceeds a threshold Th. In the muscle mechanoreflex analysis (Fig. 5*B*), the increase in CSP input induces a parallel downward shift in the MT-SNA relationship from the solid thin line to the dashed line. Because of the threshold, SNA does not respond up to ~4 kg of MT, resulting in the MT-SNA relationship shown by the solid thick line in Fig. 5*B*. In the arterial baroreflex analysis (Fig. 5*C*), the increase in MT input induces a parallel upward shift in the CSP-SNA relationship from the dashed line to the solid thick line. The observed CSP-SNA relationship at a low MT is shown as the solid thin line rather than the dashed line in Fig. 5*C* because of the threshold for SNA. Because of the subliminal fringe (gray area in Fig. 5, *B* and *C*), the response ranges of SNA for the muscle mechanoreflex and the arterial baroreflex can change depending on the input of the other reflex.

An iterative nonlinear least-squares fitting of *Eq. 3* was performed on 16 combinations of SNA data for 4 CSP levels and 4 MT levels to determine 7 parameters (P_1–P_4, A_1, A_2, and Th) in each animal. The model successfully reproduced the

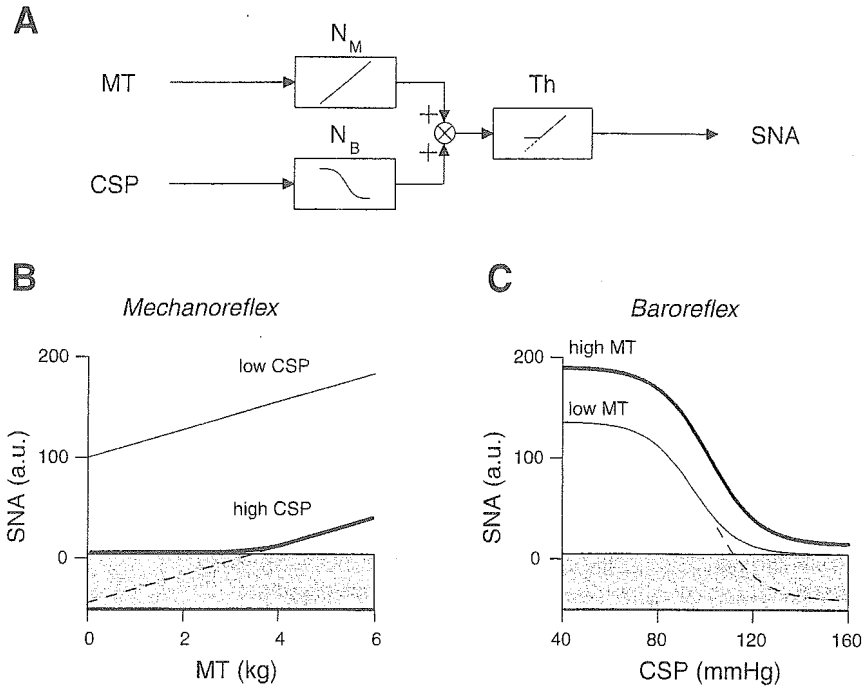

Fig. 5. Hypothetical model of interaction between the muscle mechanoreflex and the arterial baroreflex. *A*: simplified block diagram showing how the muscle mechanoreflex and the arterial baroreflex are functionally integrated based on the model of algebraic summation with a threshold (Th) (see *Functional model for interaction between muscle mechanoreflex and carotid sinus baroreflex* in DISCUSSION for details). N_M and N_B, neural arc subsystems for the muscle mechanoreflex and the arterial baroreflex, respectively. The signals derived from the muscle mechanoreflex and arterial baroreflex compartments were summed, and then the sum was compared with Th to yield SNA. *B*: muscle mechanoreflex. The increase in CSP input induces a parallel downward shift of the MT-SNA relationship from the solid thin line to the dashed line. SNA does not respond up to ~4 kg of MT because of the threshold for SNA (solid thick line). *C*: arterial baroreflex. The increase in MT input induces a parallel upward shift in the CSP-SNA relationship from the dashed line to the solid thick line. The CSP-SNA relationship at a low MT would follow the solid thin line because of the threshold for SNA.

characteristics of the interaction between the two reflexes (Fig. 6, *A* and *B*). Figure 6*C* shows the relationship between SNA estimated from the model and SNA that was actually measured. A linear regression analysis indicated that the estimated SNA in the model was similar to the measured SNA. This result reinforces our summation-threshold model of interaction between the muscle mechanoreflex and the arterial baroreflex.

Limitations. The first limitation of the present study is that we performed the experiment in anesthetized animals. Anesthesia might have modified both the carotid sinus baroreflex and the muscle mechanoreflex.

Second, we only focused on the static interaction and did not investigate the dynamic interaction between the muscle mechanoreflex and the arterial baroreflex in the present study.

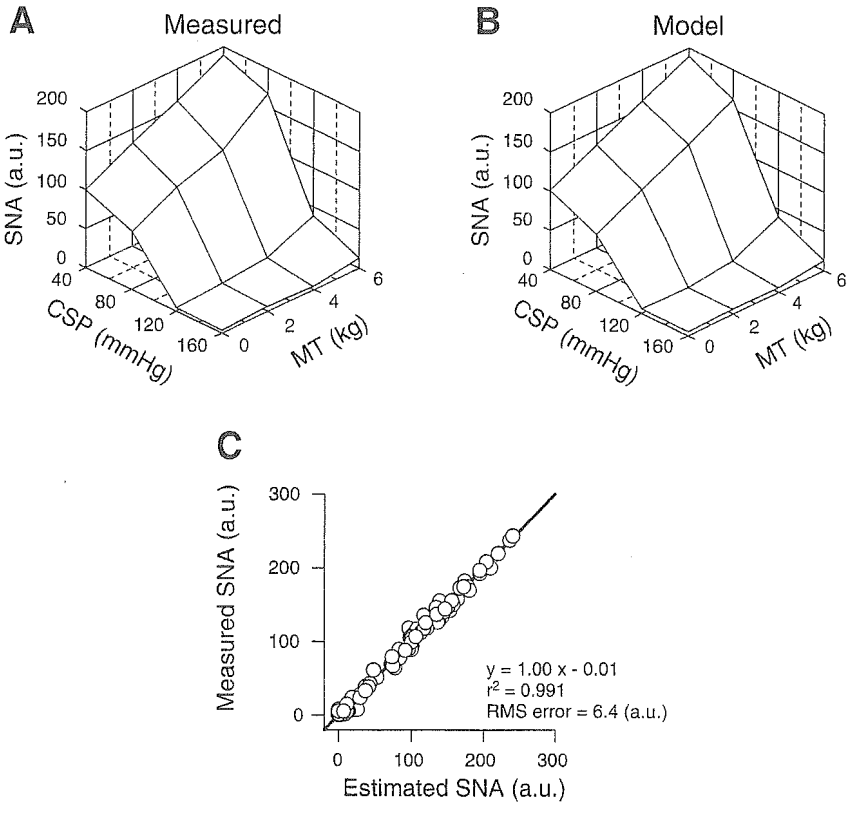

Fig. 6. *A*: averaged surface depicting the interaction between the muscle mechanoreflex and the carotid sinus baroreflex in determining SNA. *B*: surface depicting interaction, estimated by a model of algebraic summation, between the muscle mechanoreflex and the carotid sinus baroreflex with a SNA threshold. *C*: relationship between SNA estimated from the model and SNA actually measured. Each animal provided 16 data points (112 data points in total). The SNA estimated by the model was similar to the measured SNA. RMS, root mean square. Mean parameter values from *Eq. 3* least-squares fitting on SNA data are as follows: P_1, 193 a.u.; P_2, 0.10 a.u./mmHg; P_3, 101 mmHg; P_4, −54 mmHg; A_1, 15 a.u./kg; A_2, −36 a.u.; Th, 3.0 a.u., where P_1 is difference between maximum and minimum SNA; P_2 is coefficient of gain; P_3 is midpoint of logistic function on CSP axis, P_4 is SNA minimum; A_1 is slope; A_2 is intercept; and Th is SNA threshold.

Further investigations focusing on the dynamic interaction are required.

Third, stretch of skeletal muscle provides a stimulus for activation of mechanoreceptors that is different from that which occurs during muscle contraction. During contraction, mechanoreceptors are activated by a shortening of skeletal muscle and by compression of the receptors. Thus mechanoreceptors may be stimulated in a very different manner during stretch, which would likely affect the magnitude of the corresponding reflex response. In addition, stretch may activate different afferents than contraction. Further studies are required to elucidate the interactions between baroreflex and muscle mechanoreflex induced by different modes of activation.

In conclusion, activation of afferents from baroreceptors shifted the MT-SNA relationship downward and reduced the response range. The activation of mechanosensitive afferents from skeletal muscles shifted the CSP-SNA relationship upward and extended the response range. A model of algebraic summation with a threshold may explain the integration of the two reflexes. The existence of the subliminal fringe may increase the capacity of the arterial baroreflex to stabilize AP during exercise and express the sympathoexcitatory responses induced by weak muscle mechanoreceptor input at lower AP.

GRANTS

This study was supported by a Health and Labour Sciences Research Grant for Research on Advanced Medical Technology from the Ministry of Health, Labour and Welfare of Japan (H14-Nano-002), by a Grant-in-Aid for Scientific Research (A) (15200040) from the Japan Society for the Promotion of Science, and by the Program for Promotion of Fundamental Studies in Health Science of the Pharmaceuticals and Medical Devices Agency of Japan.

REFERENCES

1. **DiCarlo SE and Bishop VS.** Onset of exercise shifts operating point of arterial baroreflex to higher pressures. *Am J Physiol Heart Circ Physiol* 262: H303–H307, 1992.
2. **Gallagher KM, Fadel PJ, Stromstad M, Ide K, Smith SA, Querry RG, Raven PB, and Secher NH.** Effects of exercise pressor reflex activation on carotid baroreflex function during exercise in humans. *J Physiol* 533: 871–880, 2001.
3. **Gallagher KM, Fadel PJ, Stromstad M, Ide K, Smith SA, Querry RG, Raven PB, and Secher NH.** Effects of partial neuromuscular blockade on carotid baroreflex function during exercise in humans. *J Physiol* 533: 861–870, 2001.
4. **Hayes SG and Kaufman MP.** MLR stimulation and exercise pressor reflex activate different renal sympathetic fibers in decerebrate cats. *J Appl Physiol* 92: 1628–1634, 2002.
5. **Ichinose M, Saito M, Wada H, Kitano A, Kondo N, and Nishiyasu T.** Modulation of arterial baroreflex dynamic response during muscle metaboreflex activation in humans. *J Physiol* 544: 939–948, 2002.
6. **Iellamo F, Legramante JM, Raimondi G, and Peruzzi G.** Baroreflex control of sinus node during dynamic exercise in humans: effects of central command and muscle reflexes. *Am J Physiol Heart Circ Physiol* 272: H1157–H1164, 1997.
7. **Kaufman MP, Longhurst JC, Rybicki KJ, Wallach JH, and Mitchell JH.** Effects of static muscular contraction on impulse activity of groups III and IV afferents in cats. *J Appl Physiol* 55: 105–112, 1983.
8. **Kawada T, Zheng C, Yanagiya Y, Uemura K, Miyamoto T, Inagaki M, Shishido T, Sugimachi M, and Sunagawa K.** High-cut characteristics of the baroreflex neural arc preserve baroreflex gain against pulsatile pressure. *Am J Physiol Heart Circ Physiol* 282: H1149–H1156, 2002.
9. **Kent BB, Drane JW, Blumenstein B, and Manning JW.** A mathematical model to assess changes in the baroreceptor reflex. *Cardiology* 57: 295–310, 1972.
10. **McCloskey DI and Mitchell JH.** Reflex cardiovascular and respiratory responses originating in exercising muscle. *J Physiol* 224: 173–186, 1972.
11. **McIlveen SA, Hayes SG, and Kaufman MP.** Both central command and exercise pressor reflex reset carotid sinus baroreflex. *Am J Physiol Heart Circ Physiol* 280: H1454–H1463, 2001.
12. **Mense S and Stahnke M.** Responses in muscle afferent fibres of slow conduction velocity to contractions and ischaemia in the cat. *J Physiol* 342: 383–397, 1983.
13. **Miki K, Yoshimoto M, and Tanimizu M.** Acute shifts of baroreflex control of renal sympathetic nerve activity induced by treadmill exercise in rats. *J Physiol* 548: 313–322, 2003.
14. **Ogoh S, Wasmund WL, Keller DM, O-Yurvati A, Gallagher KM, Mitchell JH, and Raven PB.** Role of central command in carotid baroreflex resetting in humans during static exercise. *J Physiol* 543: 349–364, 2002.
15. **Potts JT, Hand GA, Li J, and Mitchell JH.** Central interaction between carotid baroreceptors and skeletal muscle receptors inhibits sympathoexcitation. *J Appl Physiol* 84: 1158–1165, 1998.
16. **Potts JT and Li J.** Interaction between carotid baroreflex and exercise pressor reflex depends on baroreceptor afferent input. *Am J Physiol Heart Circ Physiol* 274: H1841–H1847, 1998.
17. **Potts JT and Mitchell JH.** Rapid resetting of carotid baroreceptor reflex by afferent input from skeletal muscle receptors. *Am J Physiol Heart Circ Physiol* 275: H2000–H2008, 1998.
18. **Potts JT, Paton JF, Mitchell JH, Garry MG, Kline G, Anguelov PT, and Lee SM.** Contraction-sensitive skeletal muscle afferents inhibit arterial baroreceptor signalling in the nucleus of the solitary tract: role of intrinsic GABA interneurons. *Neuroscience* 119: 201–214, 2003.
19. **Rowell LB, O'Leary DS, and Kellogg DS.** Integration of cardiovascular control system in dynamic exercise. In: *Handbook of Physiology. Exercise: Regulation and Integration of Multiple Systems.* Bethesda, MD: Am. Physiol. Soc., 1996, sect. 12, chapt. 17, p. 770–838.
20. **Sato T, Kawada T, Shishido T, Sugimachi M, Alexander J Jr, and Sunagawa K.** Novel therapeutic strategy against central baroreflex failure: a bionic baroreflex system. *Circulation* 100: 299–304, 1999.
21. **Sato T, Kawada T, Sugimachi M, and Sunagawa K.** Bionic technology revitalizes native baroreflex function in rats with baroreflex failure. *Circulation* 106: 730–734, 2002.
22. **Smith SA, Querry RG, Fadel PJ, Gallagher KM, Stromstad M, Ide K, Raven PB, and Secher NH.** Partial blockade of skeletal muscle somatosensory afferents attenuates baroreflex resetting during exercise in humans. *J Physiol* 551: 1013–1021, 2003.
23. **Stebbins CL, Brown B, Levin D, and Longhurst JC.** Reflex effect of skeletal muscle mechanoreceptor stimulation on the cardiovascular system. *J Appl Physiol* 65: 1539–1547, 1988.
24. **Tallarida G, Baldoni F, Peruzzi G, Raimondi G, Massaro M, and Sangiorgi M.** Cardiovascular and respiratory reflexes from muscles during dynamic and static exercise. *J Appl Physiol* 50: 784–791, 1981.
25. **Wilson LB, Dyke CK, Pawelczyk JA, Wall PT, and Mitchell JH.** Cardiovascular and renal nerve responses to static muscle contraction of decerebrate rabbits. *J Appl Physiol* 77: 2449–2455, 1994.
26. **Yamamoto K, Kawada T, Kamiya A, Takaki H, Miyamoto T, Sugimachi M, and Sunagawa K.** Muscle mechanoreflex induces the pressor response by resetting the arterial baroreflex neural arc. *Am J Physiol Heart Circ Physiol* 286: H1382–H1388, 2004.
27. **Yanagiya Y, Sato T, Kawada T, Inagaki M, Tatewaki T, Zheng C, Kamiya A, Takaki H, Sugimachi M, and Sunagawa K.** Bionic epidural stimulation restores arterial pressure regulation during orthostasis. *J Appl Physiol* 97: 984–990, 2004.

Resetting of the arterial baroreflex increases orthostatic sympathetic activation and prevents postural hypotension in rabbits

Atsunori Kamiya[1], Toru Kawada[1], Kenta Yamamoto[1], Daisaku Michikami[1], Hideto Ariumi[1], Kazunori Uemura[1], Can Zheng[1], Syuji Shimizu[1], Takeshi Aiba[1], Tadayoshi Miyamoto[1], Masaru Sugimachi[1] and Kenji Sunagawa[2]

[1] *Department of Cardiovascular Dynamics, National Cardiovascular Centre Research Institute, Osaka, Japan*
[2] *Department of Cardiovascular Medicine, Kyusyu University Graduate School of Medical Sciences, Fukuoka, Japan*

Since humans are under ceaseless orthostatic stress, the mechanism to maintain arterial pressure (AP) under orthostatic stress against gravitational fluid shift is of great importance. We hypothesized that (1) orthostatic stress resets the arterial baroreflex control of sympathetic nerve activity (SNA) to a higher SNA, and (2) resetting of the arterial baroreflex contributes to preventing postural hypotension. Renal SNA and AP were recorded in eight anaesthetized, vagotomized and aortic-denervated rabbits. Isolated intracarotid sinus pressure (CSP) was increased stepwise from 40 to 160 mmHg with increments of 20 mmHg (60 s for each CSP level) while the animal was placed supine and at 60 deg upright tilt. Upright tilt shifted the CSP–SNA relationship (the baroreflex neural arc) to a higher SNA, shifted the SNA–AP relationship (the baroreflex peripheral arc) to a lower AP, and consequently moved the operating point to marked high SNA while maintaining AP. A simulation study suggests that resetting in the neural arc would double the orthostatic activation of SNA and increase the operating AP in upright tilt by 10 mmHg, compared with the absence of resetting. In addition, upright tilt did not change the CSP–AP relationship (the baroreflex total arc). A simulation study suggests that although a downward shift of the peripheral arc could shift the total arc downward, resetting in the neural arc would compensate this fall and prevent the total arc from shifting downward to a lower AP. In conclusion, upright tilt increases SNA by resetting the baroreflex neural arc. This resetting may compensate for the reduced pressor responses to SNA in the peripheral cardiovascular system and contribute to preventing postural hypotension.

(Resubmitted 10 March 2005; accepted after revision 29 April 2005; first published online 5 May 2005)
Corresponding author A. Kamiya: Department of Cardiovascular Dynamics, National Cardiovascular Centre Research Institute, Osaka 565-8565, Japan. Email: kamiya@ri.ncvc.go.jp

The maintenance of arterial pressure (AP) under orthostatic stress against gravitational fluid shift is of great importance, but the mechanisms remain unknown. During standing, a gravitational fluid shift directed toward the lower part of the body (such as the abdominal vascular bed and lower limbs) will cause severe postural hypotension if not counteracted by compensatory mechanisms (Rowell, 1993). Arterial baroreflexes have been considered to be the major compensatory mechanism (Persson & Kirchheim, 1991; Eckberg & Sleight, 1992; Rowell, 1993) since denervation of baroreceptor afferents causes profound postural hypotension (Sato *et al.* 2002). Earlier studies have characterized baroreflexes and their control of sympathetic nerve activity (SNA) and heart rate (Rea & Eckberg, 1987; Persson & Kirchheim, 1991; Eckberg & Sleight, 1992; Rudas *et al.* 1999; DiCarlo & Bishop, 2001; Kawada *et al.* 2003). However, the role of baroreflexes in orthostatic posture is little known. What determines AP and SNA in response to orthostatic stress remains unclear.

The baroreflex is a negative feedback control system functioning physiologically to attenuate perturbations in AP (Eckberg & Sleight, 1992; Sato *et al.* 1999). Baroreflex equilibrium diagram analysis is, to our knowledge, the best method to define the operating point (operating SNA and AP) of baroreflex (Sato *et al.* 1999). The equilibrium diagram consists of the neural and peripheral arcs. The neural arc represents the static input–output relationship between baroreceptor pressure and SNA, whereas the peripheral arc represents the relationship between SNA

DOI: 10.1113/jphysiol.2005.086512

and systemic AP. The intersection of the neural and peripheral arcs defines the operating point of AP regulation in the baroreflex closed-loop condition (for details, see Methods, Theoretical considerations: coupling of neural and peripheral arcs) (Sato *et al.* 1999; Yamamoto *et al.* 2004).

In contrast to supine posture, in orthostatic posture a gravitational body fluid shift directed toward the lower part of the body (Rowell, 1993) decreases the effective circulatory blood volume (Sagawa *et al.* 1988; Rowell, 1993). Therefore, orthostatic stress probably attenuates the pressor response to SNA in the cardiovascular system (i.e. the baroreflex peripheral arc). If orthostatic stress resets the baroreflex neural arc to augment SNA, the resetting would compensate for the attenuated pressor response of the baroreflex peripheral arc and prevent AP falling under orthostatic stress. We hypothesized that (1) orthostatic stress resets the baroreflex neural arc to a higher SNA, and (2) resetting of the arterial baroreflex contributes to preventing postural hypotension.

Methods

Theoretical considerations: coupling of neural and peripheral arcs (Fig. 1)

The arterial baroreflex is a negative feedback control system that senses AP (strictly, transmural pressure; Angell James, 1971) by baroreceptors and regulates it. When the baroreflex feedback loop is closed, baroreceptor input pressure (i.e. carotid sinus pressure; CSP) equals AP. This situation makes it difficult to analyse the behaviour of the arterial baroreflex. In this study, we used a baroreflex open-loop equilibrium diagram analysis. We opened the baroreflex loop by isolating the baroreceptor element from the systemic circulation, and changed the input baroreceptor pressure independently of systemic AP. Moreover, we measured the efferent SNA, and divided the baroreflex system into the neural arc (from baroreceptor pressure input to efferent SNA) and the peripheral arc (from SNA to AP) (Fig. 1*A*, middle panel). The neural arc is a reverse sigmoid relation and the peripheral arc is a sigmoid relation (Fig. 1*A*, top and bottom panels).

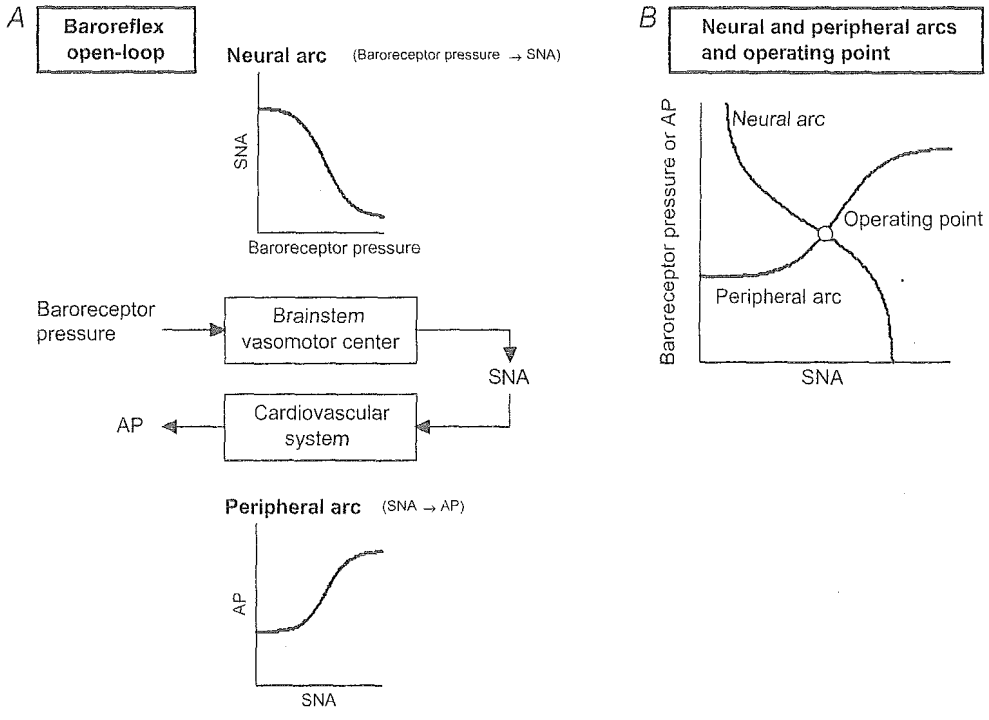

Figure 1. Theoretical considerations of the coupling of baroreflex neural and peripheral arcs
Although the baroreflex is a negative feedback control system that senses arterial pressure (AP) by baroreceptors and regulates AP, we opened the loop by changing baroreceptor pressure independently of AP (*A*). By measuring sympathetic nerve activity (SNA), we divided the baroreflex system into the neural arc (from baroreceptor pressure input to efferent SNA) and the peripheral arc (from SNA to AP) (*A*, middle panel). Both arcs show sigmoidal input–output relationships (*A*, top and bottom panels). Since baroreceptor pressure is equilibrated with AP under the baroreflex closed-loop condition, the intersection when these two arcs are superimposed defines the operating point of the baroreflex feedback system (*B*).

Importantly, baroreceptor pressure equals AP in the baroreflex closed-loop condition. Accordingly, when the two relationships are superimposed (Fig. 1*B*), the intersection of these arcs defines the operating point of the baroreflex feedback system. The validity of this framework has been confirmed in earlier studies showing that the AP and SNA estimated from the intersection agree with those measured in the closed-loop condition (Sato *et al.* 1999; Yamamoto *et al.* 2004).

Surgical preparations

Animals were cared for in strict accordance with the *Guiding Principles for the Care and Use of Animals in the Field of Physiological Science* of the Physiological Society of Japan. Eight Japanese White rabbits weighing 2.4–3.3 kg were initially anaesthetized by intravenous injection (2 ml kg^{-1}) of a mixture of urethane (250 mg ml^{-1}) and α-chloralose (40 mg ml^{-1}). Anaesthesia level were maintained by continuously infusing the anaesthetics at a rate of 0.33 ml kg^{-1} h^{-1} using a syringe pump (CFV-3200, Nihon Kohden, Tokyo). The rabbits were mechanically ventilated with oxygen-enriched room air. The bilateral carotid sinuses were isolated vascularly from systemic circulation by ligating the internal and external carotid arteries and other small branches originating from the carotid sinus regions. The isolated carotid sinuses were filled with warm physiological saline through catheters inserted via the common carotid arteries. The CSP was measured using a fluid-filled pressure transducer (AP-630G, Nihon Kohden, Tokyo) at the level of the carotid sinus throughout the experiment, and controlled by a servo-controlled piston pump (model ET-126 A; Labworks, Costa Mesa, CA, USA). In this condition, changes in carotid artery dimension are proportional to changes in carotid artery pressure. Bilateral vagal and aortic depressor nerves were sectioned at the middle of the neck to eliminate reflexes from the cardiopulmonary region and the aortic arch. Systemic AP was measured using a high-fidelity pressure transducer (Millar Instruments; Houston, TX, USA) inserted retrograde from the right common carotid artery below the isolated carotid sinus region. Body temperature was maintained at around 38°C with a heating pad. Additional injection of anaesthetics were never required as judged from haemodynamics (AP) in supine posture that were stable in the course of experiments.

We exposed the left renal sympathetic nerve retroperitoneally and attached a pair of stainless steel wire electrodes (Bioflex wire AS633; Cooner Wire, Chatworth, CA, USA) to record renal SNA. The nerve fibres peripheral to the electrodes were tightly ligated and crushed to eliminate afferent signals from the kidney. The nerve and electrodes were covered with a mixture of silicone gel (Silicon Low Viscosity, KWIK-SIL; World Precision Instrument, Inc., FL, USA) to insulate and immobilize the electrodes. The preamplified nerve signal was band-pass filtered at 150–1000 Hz, full-wave rectified and low-pass filtered with a cut-off frequency of 30 Hz to quantify the nerve activity. Pancuronium bromide (0.1 mg kg^{-1}) was administered to prevent contamination of muscular activity in the SNA recording. After all protocols were finished, animals were killed by intravenous infusion of hexamethonium bromide (6 mg kg^{-1}).

Protocols

After the surgical preparation, the animal was maintained in the supine position (0 deg) on a tilt bed. To stabilize the posture, the head was fixed full-frontal to the bed by strings, and the body and legs were rigged up in a clothes-like bag. In protocol 1, the static non-linear characteristics of the sympathetic baroreflex system were estimated in the supine position. CSP was decreased to 40 mmHg, and then increased stepwise from 40 to 160 mmHg with increments of 20 mmHg. Each CSP step was maintained for 60 s.

In protocol 2, to obtain the actual operating pressure in the baroreflex closed-loop condition in both supine and 60 deg upright positions, CSP was matched with systemic AP via the servo-controlled piston pump. The animal was kept supine for 10 min, and then tilted upright to 60 deg within 10 s by inclining the tilt bed to 60 deg and dropping the lower regions of rabbit with the fulcrum set at the level of the carotid sinus. The 60 deg upright posture was maintained for 10 min. Since the clothes-like bag stabilized the posture of the animals, there was no additional mechanical movement that reduced the quality of measurements. The position of the head remained almost fixed during the tilt to minimize vestibular stimulation.

In protocol 3, the static non-linear characteristics of the sympathetic baroreflex system were estimated during the 60 deg upright tilt. CSP was increased stepwise from 40 to 160 mmHg similar to protocol 1.

Data analysis

In protocols 1 and 3, AP and SNA were averaged during the last 10 s of each CSP level. For normalization of SNA, the noise level when animals were killed after experiments was assigned 0 arbitrary units (a.u). The mean SNA at CSP of 40 mmHg in the supine position were assigned 100 arbitrary units (a.u). Other SNA signals in both postures were normalized to these units.

The relationship between the input (CSP in the neural arc, SNA in the peripheral arc, CSP in the total arc) and

output (SNA in the neural arc, AP in the peripheral arc, AP in the total arc) is parametrically characterized by a four-parameter logistic equation model as follows (Kent *et al.* 1972):

$$y = \frac{P_1}{1 + \exp[P_2(x - P_3)]} + P_4 \quad (1)$$

where y is the output and x the input, P_1 is the response range of change in y, P_2 is the coefficient for calculating gain, P_3 is the value of x corresponding to the mid-point of operation, and P_4 is the minimum value of y. Instantaneous gain was calculated from the first derivative of the logistic function (the maximum gain equals $-P_1P_4/4$ at $x = P_3$). The intersection of the neural and peripheral arc curves on the equilibrium diagram was defined as the estimated operating point (Fig. 1), in supine and upright tilt positions. The hypothetical operating point during upright tilt (in which tilt changes the peripheral arc, but not the neural arc), was simulated by using the intersections of the supine neural arc and the upright tilt peripheral arc.

The measured operating AP and SNA of the baroreflex were obtained in protocol 2. AP and SNA were averaged during the last 3 min in the baroreflex closed-loop condition both in the supine position and with 60 deg upright tilt.

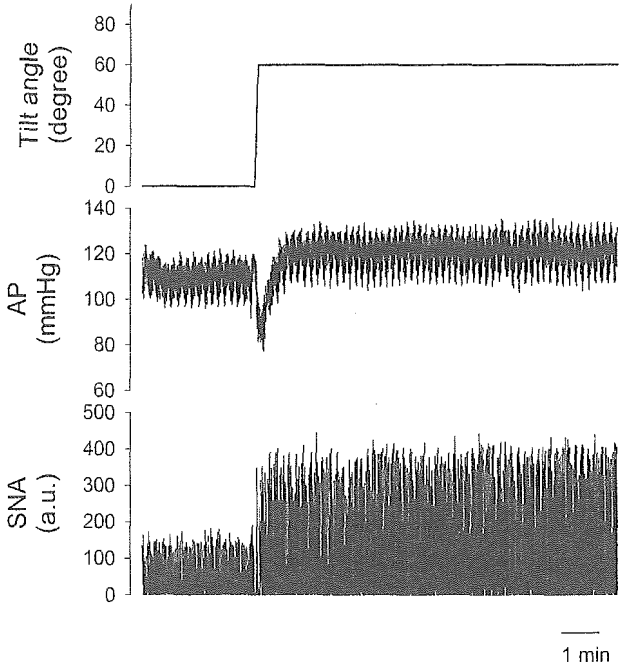

Figure 2. Time series of SNA and AP in response to a postural change from horizontal supine (3 min) to 60 deg upright tilt position (10 min)
Data were resampled at 10 Hz. The SNA and AP reach a steady state within 3 min.

Statistic analysis

All data are presented as means ± S.D. Student's paired t test was used to compare the parameters of the neural and peripheral arcs and operating points between postures (Glantz, 1997). Differences were considered significant when $P < 0.05$. A linear regression analysis was used to compare the operating points estimated from the equilibrium diagram with those measured (Glantz, 1997).

Results

Figures 2–4 show examples of data derived from the same animal. In the baroreflex closed-loop condition, 60 deg upright tilt rapidly decreased and then increased AP, and transiently decreased and then increased SNA (Fig. 2). Both AP and SNA reached nearly steady states within 3 min (Fig. 2).

In the baroreflex open-loop condition, SNA and AP decreased in response to stepwise increase in CSP both in the supine position (Fig. 3*A*) and at 60 deg upright tilt (Fig. 3*B*). In the neural arc, SNA was higher during upright tilt than supine at all CSP levels (Fig. 4*A*). The upright tilt

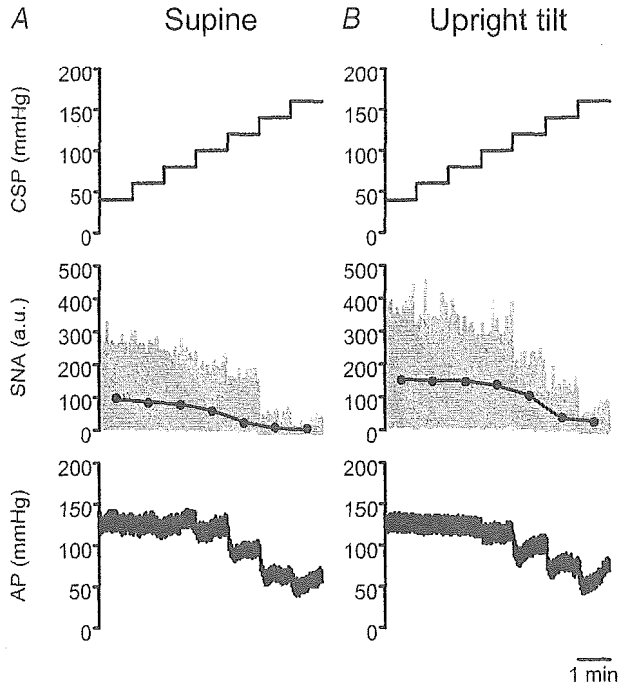

Figure 3. Time series of SNA and AP in response to stepwise increase in intracarotid sinus pressure (CSP) in supine (*A*) and 60 deg upright tilt positions (*B*)
Each CSP step was maintained for 1 min. The same animal in Fig. 2 was used in this study. Data were resampled at 10 Hz. In the middle panels, the fine vertical spikes indicate SNA signals resampled at 10 Hz, while the continuous bold line indicates data averaged over 1 min. SNA and AP decrease in response to increments in CSP for both postures. Upright tilt increases SNA at all CSP levels.

shifted the CSP–SNA curve rightward to a higher SNA. Meanwhile, in the peripheral arc, the upright tilt shifted the SNA–AP curve downward to a lower AP (Fig. 4*B*). Consequently, as the animal was changed from supine to upright tilt, the operating point estimated from the intersection of the two arcs shifted from point S to point U with a marked increase in SNA and a slight increase in AP (Fig. 4*C*). In the total arc, the upright tilt slightly steepened the CSP–AP curve, and also slightly increased the operating AP from point St to point Ut (Fig. 4*E*).

Group-averaged data show that the 60 deg upright tilt shifted the neural arc to higher SNA (Fig. 5*A*), shifted the peripheral arc to lower AP (Fig. 5*B*), and moved the operating point to markedly higher SNA (25 ± 5 a.u) while maintaining AP (Fig. 5*C*). In a simulation where 60 deg upright tilt produces no shift in the neural arc (i.e. no resetting), then the operating point during the tilt would be the intersection between the neural arc at supine and the peripheral arc at upright tilt (point A). The upright tilt would shift the operating point to a SNA (13 ± 5 a.u., Table 1) only half of that compared with when there is a neural arc shift, while the operating AP at upright tilt would decrease by 10 ± 2 mmHg.

Group-averaged data show that the 60 deg upright tilt did not change the total arc curve (Fig. 5*D*). The operating AP point in the total arc was constant during the postural change (point St overlapped with point Ut, in Fig. 5*E*). In a simulation where 60 deg upright tilt produces no shift in the neural arc (i.e. no resetting), then the tilt would shift the total arc curve downward to a lower AP (line joining crosses) and decrease the operating AP from point St to point At (Fig. 5*E*).

Group-averaged data of P_1 (the range of SNA response to CSP) and P_4 (the minimum value of SNA) in the neural arc were larger at 60 deg upright tilt than supine (Table 2). In the peripheral arc, P_1 (the range of AP response to SNA) was smaller while P_3 (midpoint of the SNA operating range) was higher at 60 deg upright tilt (Table 1). In both

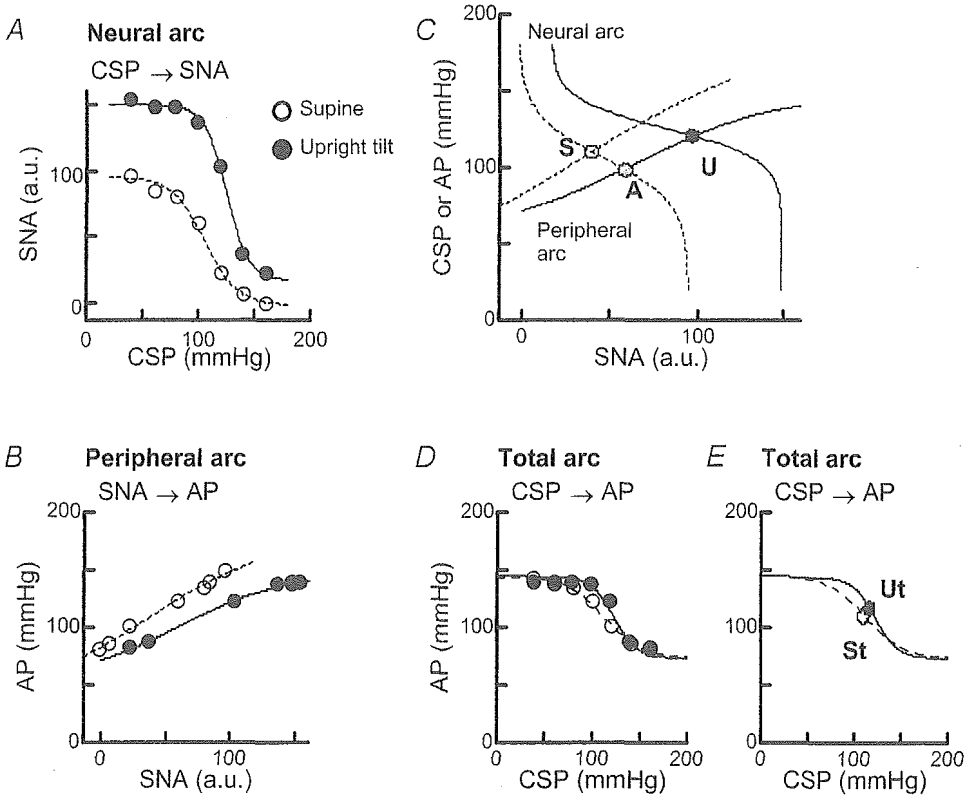

Figure 4. Example of baroreflex neural arc (*A*), peripheral arc (*B*) and total arc (*D* and *E*), and the baroreflex equilibrium diagram (*C*) in supine (○, dotted line) and 60 deg upright tilt positions (●, continuous line)

Data were obtained from the same animal as in Figs 2 and 3. The upright tilt shifts the neural arc to a higher SNA (*A*), shifts the peripheral arc to a lower AP (*B*), and moves the operating point from point S to point U (*C*). In the baroreflex equilibrium diagram (*E*), point S and U indicate the estimated operating points in supine and upright tilt positions, respectively. Point A (grey circle) indicates the estimated operating point in upright tilt position in the absence of neural arc shift (simulation) (*C*). The upright tilt slightly steepens the total arc and moves the operating AP from point St to point Ut (*D* and *E*). In the total arc (*E*), points St and Ut indicate the estimated operating points in supine and upright tilt positions, respectively.